

**DELAYED KCNQ1/KCNE1 ASSEMBLY ON THE CELL SURFACE HELPS
I_{Ks} FULFILL ITS FUNCTION AS A REPOLARIZATION RESERVE IN THE HEART**

Short title: Where are I_{Ks} channels formed in cardiomyocytes?

Zachary T. Wilson¹, Min Jiang^{1,2} Jing Geng²,
Sukhleen Kaur¹, Samuel W. Workman^{1*}, Jon Hao³, Tytus Bernas⁴, Gea-Ny Tseng¹

1. Department of Physiology & Biophysics
Virginia Commonwealth University
Richmond, VA 23298
2. Institute of Medicinal biotechnology
Chinese Academy of Medical Sciences
and Peking Union Medical College
Beijing 100050, P. R. China
3. Poochon Scientific, Frederick, MD 21703
4. Department of Anatomy & Neurobiology
Virginia Commonwealth University
Richmond, VA 23298

For correspondence:

Gea-Ny Tseng, PhD

Department of Physiology & Biophysics

Virginia Commonwealth University

Richmond, VA 23298

gea-ny.tseng@vcuhealth.org

(804)827-0811

Table of Contents category: Molecular and Cellular

* Current address: Rutgers University, School of Medicine, Piscataway, NJ 08854

KEY POINTS

- In adult ventricular myocytes, the I_{Ks} channels are distributed on the surface sarcolemma, not t-tubules.
- In adult ventricular myocytes, KCNQ1 and KCNE1 have distinct cell surface and cytoplasmic pools.
- KCNQ1 and KCNE1 traffic from the endoplasmic reticulum to plasma membrane by separate routes, and assemble into I_{Ks} channels on the cell surface.
- Liquid chromatography/tandem mass spectrometry applied to affinity-purified KCNQ1 and KCNE1 reveals novel protein interactors involved in the protein trafficking and assembly.
- Microtubule plus-end binding protein 1 (EB1) is a novel KCNQ1 interactor that can guide KCNQ1 to reach the cell surface.

ABSTRACT

The slow delayed rectifier (I_{Ks}) channels consist of KCNQ1 channel and KCNE1 regulatory subunits. I_{Ks} functions as a 'repolarization reserve' in the heart by providing extra current for ventricular action potential shortening during β -adrenergic stimulation. There have been debates as to how KCNQ1 and KCNE1 traffic in cells, where they associate to form I_{Ks} channels, and the distribution pattern of I_{Ks} channels relative to adenylate cyclase 9/yotiao important for timely I_{Ks} response to β -adrenergic stimulation. We used experimental strategies not previously applied to KCNQ1, KCNE1 or I_{Ks} , to provide new insights into these issues. 'Retention-using-selected-hook' experiments showed that newly translated KCNE1 constitutively trafficked through the conventional secretory path to the cell surface. KCNQ1 largely stayed in the endoplasmic reticulum, although dynamic KCNQ1 vesicles were observed in the submembrane region. Proteomic experiments revealed a novel KCNQ1 interactor, microtubule plus-end binding protein 1 (EB1), that guided KCNQ1 to reach cell surface. Disulfide-bonded KCNQ1/KCNE1 constructs reported preferential association after they had reached cell surface. *In-situ* proximity ligation assay (PLA) detected I_{Ks} channels in surface sarcolemma but not t-tubules of ventricular myocytes, consistent with the distribution pattern of adenylate cyclase 9/yotiao. Fluorescent protein (FP)-tagged KCNQ1 and KCNE1, in conjunction with antibodies targeting their extracellular epitopes, detected distinct cell surface and cytoplasmic pools of these proteins in cardiac myocytes. We conclude that in cardiac myocytes KCNQ1 and KCNE1 traffic by different routes to surface sarcolemma where they assemble into I_{Ks} channels. This mode of *delayed* channel assembly helps I_{Ks} fulfill its function of repolarization reserve.

Keywords: cardiac electrophysiology, repolarization reserve, protein trafficking, proteomics.

INTRODUCTION

The slow delayed rectifier (I_{Ks}) channel functions as a 'repolarization reserve' in the heart (Sarkar & Sobie, 2016). During exercise or under emotional stress, β -adrenergic tone is high and heart rates are fast. More repolarizing currents are needed to shorten ventricular action potentials, to allow sufficient diastole for ventricular filling. I_{Ks} responds to β -adrenergic stimulation by becoming larger (amplitude response) and activating faster (gating response) (Marx *et al.*, 2000). As such, I_{Ks} provides the extra current needed for action potential shorting during high β -adrenergic tone (Jost *et al.*, 2005; Banyasz *et al.*, 2014).

I_{Ks} channel has two major components: a voltage-gated KCNQ1 channel and regulatory KCNE1 subunits (Sanguinetti *et al.*, 1996; Xu *et al.*, 2013). Loss-of-function mutations in KCNQ1 and KCNE1 have been linked to long QT syndrome types 1 and 5, while gain-of-function mutations in KCNQ1 have been linked to short QT syndrome type 2 (Splawski *et al.*, 2000; Borggrefe *et al.*, 2005). Excessive I_{Ks} has been observed in atrial myocytes from patients of chronic atrial fibrillation (Caballero *et al.*, 2010). These clinical data indicate the importance of a dynamic control of I_{Ks} current amplitude to support its role of 'repolarization reserve', yet preventing excessive I_{Ks} when not needed. Although the issues of how KCNQ1 and KCNE1 traffic and interact in cells have been studied for many years, there remain debates among investigators and discrepancies among reports. These debates or discrepancies are described below, in the context of four major questions we address in this study. We used experimental approaches not previously applied to the studies of KCNQ1, KCNE1 and I_{Ks} , thus providing new insights into the issues under debates.

First, where are I_{Ks} channels located in adult ventricular myocytes? To achieve a timely response to β -adrenergic stimulation, cell surface I_{Ks} channels need to be close to adenylate cyclase 9 (AC9) and yotiao (also known as A-kinase anchoring protein 9). This is because I_{Ks} response to β -adrenergic stimulation relies on cAMP production by AC9 (Li *et al.*, 2019), and recruitment of protein kinase A (PKA) and protein phosphatase 1A (PP1A) by yotiao to its vicinity (Marx *et al.*, 2000). It has been shown that in adult mouse ventricular myocytes, AC9 and yotiao both cluster to the surface sarcolemma (SS) but not t-tubules (TT) (Li *et al.*, 2019). Yet it has been proposed that KCNQ1, and likely the I_{Ks} channels, are highly enriched in t-tubules instead of surface sarcolemma (Rasmussen *et al.*, 2003; Balse *et al.*, 2012) (Oliveras *et al.*, 2020). Therefore, there appears to be a discrepancy between AC9/yotiao and I_{Ks} channels in terms of their subcellular distribution pattern. A common caveat in previous studies is the use of immunofluorescence of KCNQ1 and KCNE1 and their colocalization to infer I_{Ks} location (Jiang *et al.*, 2017; Oliveras *et al.*, 2020). In this study, we used a much more stringent approach, *in situ* proximity ligation assay (PLA) (Soderberg *et al.*, 2008), to detect KCNQ1/KCNE1 assembly in adult ventricular myocytes.

Second, are there separate (cell surface and cytoplasmic) pools of KCNQ1 and KCNE1 in adult ventricular myocytes? If yes, where are they? Previously, we used biochemical experiments to propose that in guinea pig hearts native KCNQ1 is mainly in a cytoplasmic compartment (in junctional sarcoplasmic reticulum, jSR), while native KCNE1 is mainly in the sarcolemma (SL) (Jiang *et al.*, 2017). Such segregation of KCNQ1 and KCNE1 into different subcellular compartments appears contradicting the conventional view that KCNQ1 and KCNE1 should be well colocalized because they are obligate partners in cardiac myocytes. Here we used antibodies binding extracellular epitopes on KCNQ1 and KCNE1 to distinguish cell surface KCNQ1 and KCNE1 from their cytoplasmic counterparts.

Third, how do KCNQ1 and KCNE1 traffic from endoplasmic reticulum (ER, where they are translated) to the cell surface, and how do they interact with each other during the journey? Previously, we proposed that KCNQ1 and KCNE1 traffic by separate routes from ER to the sarcolemma in adult ventricular myocytes (Jiang *et al.*, 2017). This concept appears at add with the view that KCNE1 requires KCNQ1 to reach cell surface (Chandrasekhar *et al.*, 2006), or KCNE1 regulates KCNQ1 trafficking to cell surface (Krumer *et al.*, 2004). One major challenge in mapping proteins' trafficking routes is the synchronization of their movements in cells. In this study, we used a novel approach 'retention using selected hook' or RUSH (Boncompain *et al.*, 2012) to synchronize the timing of KCNQ1 and KCNE1 exit from the ER. This allowed us to track their trafficking paths and timing of reaching different cellular compartments.

Fourth, where are KCNQ1 and KCNE1 assembled into I_{Ks} channels? Different scenarios have been proposed: KCNQ1 and KCNE1 assemble early while they are in the ER (Bas *et al.*, 2011), in a post-ER but pre-Golgi vesicular compartment (Vanoye *et al.*, 2010), at the Golgi (David *et al.*, 2013), or at the

ER/plasma membrane junctions (Oliveras *et al.*, 2020). In this study, we used a reporter of functional KCNQ1/KCNE1 assembly to quantitatively compare the degree of their assembly under the control conditions vs when they were forced to stay inside cells.

Finally, we used affinity purification followed by liquid chromatography/tandem mass spectrometry (LC/MS-MS) to search for novel KCNQ1 and KCNE1 interactors in cells. The proteomic data support our experimental findings: KCNQ1 and KCNE1 traffic by separate routes from ER to the surface membrane, and they cluster to the same subdomains in surface membrane to assemble into I_{Ks} channels. We also verified a novel KCNQ1 interactor identified by proteomics, microtubule plus-end binding protein 1 (EB1), that appears to guide and facilitate KCNQ1 to reach the surface membrane.

MATERIALS AND METHODS

Molecular constructs

The following plasmids were from AddGene: Str-Ii_VSVG-SBP-EGFP (from Franck Perez, Addgene plasmid # 65300) (Boncompain *et al.*, 2012), DsRed2-ER-5 (from Michael Davidson, Addgene plasmid # 55836), pECFP-SEC31A (from David Stephens, Addgene plasmid # 66612), pMXs-IP spGFP-ERGIC53 (from Noboru Mizushima, Addgene plasmid # 38270), and EB1-tdTomato (from Erik Dent, Addgene plasmid # 50825).

KCNQ1-GFP (Q1-GFP), with eGFP fused to the C-terminus of the 676 aa KCNQ1 isoform 1, was a gift from Andrew Tinker (Mashanov *et al.*, 2010). KCNE1-dsR (E1-dsR) has been described previously (Jiang *et al.*, 2017). HA-KCNE1-dsR (HA-E1-dsR) was created by inserting an HA epitope (YPYDVPDYA) between aa 20 and 21 in the extracellular domain of E1-dsR. KCNQ1-Q147C (Q1-Q147C) had glutamine at position 147 mutated to cysteine in a cysteine-removed 548 aa KCNQ1 isoform 0 background. KCNE1-G40C (E1-G40C) had glycine at position 40 of KCNE1 mutated to cysteine. Q1-Q147C and E1-G40C have been described previously (Wang *et al.*, 2011). All in-house mutations were created using Q5 Site-directed mutagenesis kit, and confirmed by direct DNA sequencing.

The ER-hooked HA-E1-dsR and ER-hooked Q1-GFP were created using Str-Ii_VSVG-SBP-EGFP as the starting material by GenScript. Str-Ii_VSVG-SBP-EGFP has an ER-membrane embedded protein (Ii, an isoform of the human invariant chain of the major histocompatibility complex with an N-terminal arginine-based motif retaining it in the ER), a core streptavidin peptide (Str) fused to its N-terminus in the cytosolic side of the ER membrane, an internal ribosome entry (IRE) sequence, followed by wild-type vesicular stomatitis virus protein G (VSVG) fused with streptavidin binding peptide (SBP) and eGFP. Q1-GFP was fused with SBP and a 7 Gly peptide in between to allow free SBP binding to Str. HA-E1-dsR was fused with SBP and a 7-Gly peptide in between. For both, Asc I and Pac I enzyme sites were created at 5' and 3' ends, respectively. The VSVG-SBP-EGFP was removed from plasmid 65300 using Asc I and Pac I cuts, followed by directed subcloning of the Q1-GFP-SBP or HA-E1-dsR-SBP to create the ER-hooked Q1-GFP and ER-hooked HA-E1-dsR constructs under CMV promoter for mammalian cell expression. Both constructs were confirmed by DNA sequencing.

Adenovirus production

HA-E1-dsR and Q1-GFP were subcloned into Adeno_shuttle vector and, after confirming gene function by patch clamp, immunoblotting, and imaging experiments, they were sent to Vector Biolabs for adenoviral production into adenoviral-type 5, $\Delta E1/E3$. The viral titers were 4.5×10^{10} and 5×10^{10} PFU/ml, respectively, where PFU stands for 'plaque formation units'.

Cardiac myocyte isolation, culture and adenovirus transduction

The investigation conformed to the Guide for the Care and Use of Laboratory Animals published by the National Institutes of Health. The animal protocol (AM10294) has been reviewed and approved annually by the Institutional Animal Care and Use Committee of Virginia Commonwealth University.

The procedures of myocyte isolation, culture, and adenovirus incubation have been described in our publication (Jiang *et al.*, 2017). Briefly, myocytes were isolated from guinea pig or Sprague Dawley rats, 2-4 month old, male, using enzymatic (collagenase, type II, Worthington) digestion, followed by mechanical trituration. Ventricular tissue chunks were gently shaken in Kraftbrue medium (KB) medium to release single myocytes. Myocytes were allowed to recover in KB for 1 hr at room temperature (RT), and switched to nominally Ca free Tyrode's (in mM: NaCl 146, HEPES 5, dextrose 10, KCl 8, pH 7.3) supplemented with BDM (5 mM), L-carnitine (2 mM), taurine (5 mM), glutamate (2 mM) and BSA (1%) for 1 hr at RT. Myocytes were plated on mouse laminin-coated coverslips or dishes and incubated in medium 199 supplemented with creatine (5 mM), L-carnitine (5 mM), taurine (5 mM), BSA (0.2%), FCS (5%), cytochalasin D (0.2 μ M), and penicillin/streptomycin, in 36°C CO₂ moist incubator. After culture for 2 hr, adenovirus was added to the culture medium at 10⁷ PFU/ml final concentration. Incubation with adenovirus continued for specified amounts of time (noted in text or figure legends), before experiments.

COS-7 and HEK293 cell culture and transfection

The procedures have been described in our previous publication (Jiang *et al.*, 2017). Briefly, cells were maintained in DMEM supplemented with 10% FCS, non-essential amino acids, penicillin and streptomycin in 36°C CO₂ moist incubator. Cells were plated on matrigel-coated coverslips or dishes, and when reaching ~70% confluency, transfected with cDNAs facilitated by lipofectamine 2000 for 5-6 hr in base DMEM. After removing cDNAs, cells were cultured in complete DMEM for 24-36 hr before experiments.

Patch clamp experiments

Currents from COS-7 cells transfected with specified cDNAs, or native currents of guinea pig ventricular myocytes, were recorded using the whole-cell patch clamp mode. COS-7 cells were superfused with normal Tyrode's solution (in mM: NaCl 146, dextrose 5.5, MgCl₂ 0.5, KCl 4, CaCl₂ 2, HEPES 5, pH 7.3) at room temperature (RT). Guinea pig ventricular myocytes were superfused with Na- and Ca-free Tyrode's solution (NaCl and CaCl₂ replaced by equimolar choline-Cl and MgCl₂) at 33°C. Patch pipette solution contained (in mM): K-aspartate 120, KCl 20, EGTA 10, ATP (K) 10, MgCl₂ 1, HEPES 10, pH 7.3. Command voltage and current recording were controlled by Clampex of pClamp 10 via Axopatch 200B/1440A interface and low-pass filter (cut off 10 kHz). Currents were analyzed with Clampfit. Numerical data were exported to Excel or SigmaPlot for processing and graph production.

In situ proximity ligation assay (PLA) experiments

The subcellular distribution pattern of KCNQ1/KCNE1 assembly was detected using in situ PLA (Soderberg *et al.*, 2008). Myocytes transduced with Q1-GFP and HA-E1-dsR and cultured for 24-36 hr were fixed (4% paraformaldehyde in PBS, at RT, 10 min), permeabilized (0.1% triton X-100 in PBS, at RT, for 10 min), and incubated with GFP mouse Ab and dsR rabbit Ab overnight at 4°C. After removing the Abs, the PLA procedure was performed using DUO92-14 kit (Sigma Aldrich) following manufacturer's instructions. Far red fluorophore was incorporated to mark sites of proximity (\leq 40 nm) between GFP mouse and dsR rabbit Abs. After the PLA procedure, the myocytes were incubated with Alexa488 donkey anti-mouse and Alexa568 donkey anti-rabbit to detect total pools of Q1-GFP and HA-E1-dsR, respectively.

Retention using selected hook (RUSH) experiments

The 'RUSH' method was designed to track protein trafficking after they are released from the domain-resident hook (Boncompain *et al.*, 2012). In our case, we used ER_hook. COS-7 cells transfected with ER-hooked constructs were cultured under the control conditions for 36 hr. Then biotin was added to the medium (final concentration 100 μ M) and incubation continued at 36°C in CO₂ moist incubator for specified amounts of time (noted in text or figure legends). Biotin competed off Str-Ii binding to SBP on the Q1-GFP, HA-E1-dsR or VSVG-GFP, releasing them from the ER hook. After biotin incubation, cells were fixed for imaging experiments. GFP and dsR were labeled with GFP goat Ab/Alexa488 donkey anti-goat and dsR rabbit Ab/Alexa568 donkey anti-rabbit, respectively.

Immunoblot experiments

Unless otherwise noted, immunoblot experiments were run under reducing conditions. Protein samples were mixed with 2x or 5x sample buffer containing reducing agent (5% mercaptoethanol), and incubated at 50°C for 15 min before loading polyacrylamide gel. Proteins were fractionated by sodium dodecylsulfate/polyacrylamide gel electrophoresis (SDS-PAGE). Proteins were transferred to PVDF membranes. The membranes were blocked by incubation in 1x TBST with 10% nonfat dry milk and then incubated with primary Abs diluted in 1xPBS with 5% BSA (4°C overnight, or 2 hr at RT). Membranes were then incubated with horse radish peroxidase (HRP)-conjugated secondary Ab and immunoreactive bands were visualized with enhanced chemiluminescence kit using an imager FluorChem M. Band intensities were quantified using AlphaView SA, and numerical data were exported to Excel for processing.

Quantification of cell surface KCNQ1 by biotinylation

To biotinylate cell surface proteins, live COS-7 cells expressing Q1-Q147C/E1-G40C were incubated with membrane-impermeable, amine-reactive biotin (EZ-Link Sulfo-NHS-SS-Biotin) at 0.25 mg/ml, for 30 min at 4°C. Biotinylation reaction was quenched by 100 mM glycine in PBS. The cells were lysed in 1% Triton X-100 lysis buffer and 90% of the whole cell lysate (WCL) was incubated with neutravidin beads to bind biotinylated (cell surface) proteins. The other 10% WCL and the eluent from neutravidin beads (biotinylated fraction) were fractionated by SDS-PAGE, and probed with an Ab targeting KCNQ1. KCNQ1 band intensities in the WCL lane (W) and in the biotinylated fraction lane (b) were quantified by densitometry, and the results were used to calculate % KCNQ1 on the cell surface: $[b/(W*9+b)]*100\%$.

Quantification of disulfide bonded Q1-Q147C/E1-G40C

COS-7 cells transfected with Q1-Q147C/E1-G40C were cultured for 24 hr at 16°C to allow protein translation without ER exit. The medium was switched to 36°C and culture continued under the control conditions, or in the presence of brefeldin A (BFA, 25 μ g/ml) for 24 hr before experiments. Cells were lysed. WCL was divided into two equal aliquots. One incubated with dithiothreitol (DTT, 50 mM, RT, 30 min) to break disulfide bonds and the other not (+DTT and -DTT). WCLs were mixed with 2x sample buffer without mercaptoethanol, and fractionated on SDS-PAGE. After proteins were transferred to PVDF membrane, the membrane was probed with an Ab targeting KCNQ1.

Microscopy experiments and image data analysis

To image fixed COS-7 cells or myocytes, cells were plated on matrigel- or laminin-coated no. 1.5 coverslips, and transfected or transduced as specified in text or figure legends. For experiments testing cell surface proteins, live COS-7 cells or fixed but un-permeabilized myocytes were incubated with antibodies targeting epitopes in the extracellular domains of KCNQ1 and KCNE1, followed by Alexa-conjugated secondary Ab targeting the surface-bound primary Ab. COS-7 cells were then fixed. COS-7

cells or myocytes were permeabilized (0.1% Triton X-100 in PBS, RT, 10 min), and incubated with Abs targeting intracellular epitopes. Coverslips were mounted on glass slides with ProLong Diamond anti-fade mountant (Molecular probes).

To image live COS-7 cells, cells were plated on matrigel-coated no. 1.5 glass-bottom microwell dishes (MatTek), transfected as described in text. Nuclei were stained with Hoechst dye. Cells were imaged in phenol red-free DMEM with 5% FCS at 37°C.

Imaging experiments were done using Zeiss 710 (confocal microscopy, diffraction-limited), Zeiss 880 (Airyscan microscopy, xy resolution improved ~ 1.7 fold), or Nikon structured illumination microscopy (SIM, xy resolution improved ~ 2 fold). COS-7 and myocytes were imaged using x63 and x40 oil immersion objectives, respectively. Fluorophores were sequentially excited by Laser lines: 405 nm (Hoechst dye), 488 nm (GFP or Alexa488), 561 nm (dsRed or Alexa568), and 633 nm (Alexa647). The emitted lights were collected with appropriate band-pass or long-pass filters to avoid 'bleed through'.

Immunoprecipitation experiments

HEK293 cells transfected with Q1-GFP and HA-E1-dsR or untransfected HEK293 cells (as negative control), or rat ventricular myocytes transduced with Q1-GFP and HA-E1-dsR were used for immunoprecipitation experiments. Whole cell lysate (WCL) in 1% Triton X-100 lysis buffer was precleared with protein A/G coated magnetic beads. The beads were collected as negative control ([-] IP) for rat ventricular myocytes. Precleared WCL was divided into equal aliquots, and each aliquot was incubated with fresh protein A/G coated magnetic beads with immunoprecipitating Abs (specified in text or figure legends) overnight at 4°C. The beads were collected as positive [+] IP. [-] and [+] IP beads were washed, and bound proteins were eluted by 2x sample buffer with 5% mercaptoethanol, at 50°C for 30 min. [-] and [+] IP were fractionated side-by-side with WCL (as direct input) by SDS-PAGE, followed by transfer to PVDF membranes. The membranes were probed with Abs noted in text or figure legends.

Proteomic experiments and data analysis

Nine immunoprecipitate samples ([+]: 2 GFP rabbit, 2 GFP goat, 2 dsR rabbit Ab from WCL of HEK293 cells transfected with Q1-GFP and HA-E1-dsR, and [-]: 1 each of GFP rabbit, GFP goat, dsR rabbit Ab from WCL of untransfected HEK293 cells) were quality checked and subject to protein identification using liquid chromatography/tandem mass spectrometry (LC/MS-MS, by Poochon Scientific). The samples were fractionated by 4-12% SDS-PAGE, followed by in-gel trypsin digestion. Tryptic peptide mixtures were cleaned up with C18 Zip-tip, and analyzed by LC/MS-MS using a Thermo Scientific Q-Exactive hybrid Quadrupole-Orbitrap Mass Spectrometer and a Thermo Dionex UltiMate 3000 RSLCnano System. Peptide mixture was loaded onto a peptide trap cartridge at a flow rate of 5 ul/min. The trapped peptides were eluted onto a reverse-phase PicoFrit column (New Objective, Woburn, MA) using a linear gradient of acetonitrile (3-36%) in 0.1% formic acid. The elution time was 60 min, at a flow rate of 0.3 ul/min. Eluted peptides were ionized and sprayed into the mass spectrometer, using a Nanospray Flex Ion Source ES071 (Thermo) under the following settings: spray voltage 1.8 kV, capillary temperature 250°C. Raw data files were searched against the Uniprot human protein database using the Proteome Discoverer 1.4 software based on the SEQUEST algorithm. Carbamidomethylation (+57.021 Da) of cysteines was a fixed modification, and oxidation of methionine and deamidation of glutamine and asparagine (+0.98402 Da) were set as dynamic modifications. The minimum peptide length was specified to be 5 amino acids. The precursor mass tolerance was set to 15 ppm, whereas the fragment mass tolerance was set to 0.05 Da. The maximum false peptide discovery rate was specified as 0.01. The resulting Proteome Discoverer Report contains all assembled proteins with peptide sequences and peptide spectrum match counts (#PSM).

The protein lists in combined GFP rabbit and goat Ab immunoprecipitate samples (4) and in DsRed rabbit Ab immunoprecipitate samples (2) were analyzed in the following manner:

- 1) The #PSM of all [+] samples were combined (Σ PSM of [+]). Those with Σ PSM of [+] ≥ 2 were retained.
- 2) Of the above, those absent in [-] (Σ PSM of [-] = 0) and those having ratio of Σ PSM ([+]/[-]) ≥ 2 were retained. There were a total of 109 proteins in GFP Ab IP (Table 1 in Appendix), and 109 proteins in dsRed Ab IP (Table 2).
- 3) The two protein lists were compared and divided into three lists: shared, KCNQ1-GFP unique and HA-KCNE1-dsR unique. These proteins were manually curated based on molecular function and/or cellular compartment.

Antibodies and reagents

Primary Abs used were: HA mouse Ab (MMS-101P, Covance), dsRed rabbit Ab (catalog # 632496, Clontech), KCNQ1 rabbit Ab targeting the extracellular domain of KCNQ1 (APC-168, Alomone), KCNQ1 goat Ab (C20, Santa Cruz biotechnology), GFP goat Ab (ab5450, AbCam), GFP rabbit Ab (ab290, AbCam), GFP mouse Ab (MA5-15256, Thermo Fisher), and EB1 rat Ab (ab53358, AbCam). Alexa-conjugated secondary Abs and WGA were purchased from Molecular Probes. HRP-conjugated secondary Abs were from Thermo Fisher.

Statistical analysis

All group data are reported by dot plots superimposed on bar graph of Mean \pm SD. Comparison between two groups was by two-tailed t-test assuming unequal variance (Excel). Comparison among more than two groups was by one-way ANOVA (SigmaStat v. 4.0). If p value was < 0.01 , this was followed by Tukey's pairwise tests. A p value < 0.05 is considered significant.

RESULTS

Fluorescent protein (FP)- and epitope-tagged KCNQ1 and KCNE1 behave like their native counterparts in adult ventricular myocytes

We used Q1-GFP and HA-E1-dsRed (details in 'Molecular constructs' of Methods) as KCNQ1 and KCNE1 surrogates. These FP-tagged constructs offered two major advantages: allowing us to observe their distribution without antibodies, and serving as a positive control (vs myocytes or cells without gene transfer) in the validation of experimental strategies. Fig. 1A shows that Q1-GFP and HA-E1-dsR expressed in rat ventricular myocytes had distribution patterns similar to those of their native counterparts in guinea pig ventricular myocytes (Fig. 1C): Q1-GFP was in prominent transverse striations, while HA-E1-dsR was prominent on the lateral surface (XY plane views). The two overlapped sporadically on or close to the lateral surface (XZ cross-sectional views) and in the intercalated disc region at cell ends. Furthermore, patch clamp of COS-7 cells expressing Q1-GFP and HA-E1-dsR revealed prominent I_{Ks} current, similar to the native I_{Ks} recorded from guinea pig ventricular myocytes (Fig. 1B and 1D).

These observations support the validity of using Q1-GFP and HA-E1-dsR to investigate how native KCNQ1 and KCNE1 traffic and interact in ventricular myocytes. We used adult rat ventricular myocytes as the expression system. They have low background KCNQ1 and KCNE1 expression (Wu *et al.*, 2006; Jiang *et al.*, 2017; Oliveras *et al.*, 2020), and their sarcolemma has distinct subdomains (t-tubule 'TT', surface sarcolemma 'SS', and intercalated disc 'ICD') important for data interpretation.

I_{Ks} channels are mainly present in the surface sarcolemma but not t-tubules in adult ventricular myocytes

We used *in situ* proximity ligation assay (PLA) (Soderberg *et al.*, 2008) to locate functional Q1-GFP and HA-E1-dsR assemblies in adult ventricular myocytes. Fig. 2A depicts the PLA procedure. The cell

membrane was permeabilized, allowing the primary antibodies, GFP mouse Ab and dsRed rabbit Ab, to bind to their FP targets in the cytoplasmic compartment. Then cells were incubated with nucleotide-conjugated PLA probes, that bound to the primary Abs. If the two primary Abs were ≤ 40 nm apart, the nucleotides could be ligated and allowed an amplification reaction. The amplification reaction incorporated fluorophore to mark the sites of proximity between the two primary Abs, allowing detection by fluorescence microscopy. In a functional Q1-GFP/HA-E1-dsR assembly, the distance between GFP mouse Ab and dsR rabbit Ab is estimated to be ≤ 37 nm, based on: (1) The cryoEM structure of KCNQ1/KCNE3 assembly (6V01.pdb), (Sun and MacKinnon (2020), which is similar to the KCNQ1/KCNE1 assembly in having KCNE3 occupying the cleft spaces between KCNQ1 subunits (Xu *et al.*, 2013). In this cryoEM structure, the C-termini of KCNQ1 and KCNE3 are ~ 7 nm apart. (2) The dimensions of eGFP (2Y0G.pdb) and monomer dsRed (2VAD.pdb) (long-axes ~ 5 nm). (3) The length of antibodies (~ 10 nm).

Fig. 3 shows that no PLA signals were detected in control myocytes (not incubated with adenoviruses) or when only Q1-GFP was expressed. PLA signals were detected when both Q1-GFP and HA-E1-dsR were expressed. The higher the expression level, the stronger the PLA signals (36 vs 24 hr culture of adenovirus-transduced myocytes). These data indicate that non-specific probe binding or non-specific nucleotide ligation was minimal.

To have a complete view of the distribution pattern of PLA signals and their relationship to Q1-GFP and HA-E1-dsR, we acquired z-stack images of the their fluorescence signals in every myocyte studied (8 myocytes, from 2 independent experiment). To quantify their distribution on lateral surface vs in cell interior (including t-tubules and cytoplasmic compartments), we collapsed the 3D z-stacks into 2D images by z-stack projection of maximal signals. The top and bottom slices were not included to avoid interference from signals on the top and bottom cell surfaces. A representative example is depicted in Fig. 2B. The PLA signals were mainly localized to the lateral surface. On the other hand, there were abundant Q1-GFP and HA-E1-dsR signals in the cell interior. This distinction offers another support for the specificity of PLA signals: PLA detected Q1-GFP/HA-E1-dsR assemblies, but not unassembled Q1-GFP and HA-E1-dsR even when they were abundant and close to each other.

We quantified the percentage of signals in the cell periphery, defined as a space 2 μ m wide within the cellular contour. Data summarized in Fig. 2C confirms the consistency of images presented in Fig. 2B: PLA signals were much more abundant in cell periphery than Q1-GFP or HA-E1-dsR. Clustering of PLA signals to the lateral surface, without transverse striation pattern in cell interior, indicates that I_{Ks} channels are mainly localized to the surface sarcolemma, instead of t-tubules. This distribution pattern is consistent with proximity between cell surface I_{Ks} channels and AC9 and yotiao (Li *et al.*, 2019), which is important for a timely I_{Ks} response to β -adrenergic stimulation.

Cell surface KCNQ1 and KCNE1 are on the surface sarcolemma but not t-tubules, and there are distinct cytoplasmic pools of KCNQ1 and KCNE1 in adult ventricular myocytes

We used a Q1 rabbit Ab that targets aa 284-297 in the extracellular domain of KCNQ1 (termed 'Q1 ext Ab') to label cell surface Q1. To test its ability and specificity in detecting cell surface targets, we exposed live COS-7 cells transiently transfected with Q1-GFP to the Q1 ext Ab, followed by Alexa-conjugated secondary Ab. Fig. 4A depicts two adjacent COS-7 cells, one expressing Q1-GFP (cell 1) and the other not (cell 2). Immunofluorescence signals of Q1 ext Ab (Q1 ext Ab IF) was clearly detected as puncta in the periphery of cell 1. No Q1 ext Ab IF was detected in cell 2. We used HA mouse Ab to detect cell surface HA-E1-dsR. Fig. 4B shows that no immunofluorescence signal of HA mAb (HA Ab IF) was detectable in myocytes not transduced with HA-E1-dsR, confirming its specificity.

Fig. 5Aa shows that in myocytes expressing Q1-GFP, the total pool of this protein detected by GFP fluorescence signals (GFP FP) showed the typical pattern of transverse striations. There were also strong perinuclear GFP signals, representing high translation activity in the nuclear envelope after adenovirus-

mediated gene transfer. Cell surface Q1-GFP was detected by incubating unpermeabilized myocytes to Q1 ext Ab, followed by Alexa-conjugated secondary Ab. Cell surface Q1-GFP was mainly in myocyte periphery. There were no perinuclear signals or striations in myocyte interior. The fluorescence profiles across the unpermeabilized myocyte in Fig. 5Ba show clear distinction between cell surface and total pools of Q1-GFP. We used the fluorescence profiles to quantify the percentage of signals in cell periphery. Data summary in Fig. 5Ca supports the consistency among myocytes: the % of Q1 ext Ab IF in cell periphery was much higher than that of GFP FP.

Exposing permeabilized myocytes to Q1 ext Ab revealed that the distribution patterns of Q1 ext Ab IF and GFP FP were qualitatively the same: strong transverse striations and perinuclear signals. This is supported by the fluorescence profiles in Fig. 5Ba. These observations confirm that cell surface Q1-GFP is on surface sarcolemma but not t-tubules. The prominent transverse striation pattern seen in total Q1-GFP (as well as immunofluorescence of native KCNQ1 in guinea pig ventricular myocyte, Fig. 1C) represents a cytoplasmic protein pool. The most likely candidate for the cytoplasmic location is the junctional SR, which is adjacent to the z-lines and cannot be distinguished from t-tubules at the light microscopy level. Cytoplasmic pool in jSR is consistent with our previous biochemical experiments on native KCNQ1 in guinea pig heart (Jiang *et al.*, 2017).

Fig. 5Ab shows that in myocytes expressing HA-E1-dsR, the total protein pool detected by the dsRed fluorescence (dsRed FP) had the typical distribution pattern: prominent on lateral surface and in vesicles, and dim in striations. Cell surface HA-E1-dsR was labeled by exposing unpermeabilized myocytes to HA mAb followed by Alexa-conjugated secondary Ab. Cell surface HA-E1-dsR was exclusively on the surface sarcolemma. There were no striations or vesicles. The fluorescence profiles across the myocyte width support the clear distinction between dsRed FP and HA Ab IF in the unpermeabilized myocyte (Fig. 5Bb). Data summary in Fig. 5Cb supports the consistency among myocytes: the % of HA Ab IF in cell periphery was much higher than that of dsRed FP. Exposing permeabilized myocytes to the HA Ab showed that the distribution patterns of HA Ab IF and dsRed FP overlapped (Fig. 5Ab and 5Bb). Therefore, similar to Q1-GFP, cell surface HA-E1-dsR is on surface sarcolemma but not t-tubules. The dim transverse striation pattern seen in total HA-E1-dsR represents a cytoplasmic pool, possibly the jSR as is the case for Q1-GFP.

KCNQ1 and KCNE1 traffic through separate routes from endoplasmic reticulum to the plasma membrane

We used a strategy 'retention using selective hook', or RUSH (Boncompain *et al.*, 2012), to synchronize ER exit of Q1-GFP and HA-E1-dsR. This allowed us to monitor their paths and time courses of forward trafficking. The molecular construct and experimental protocol of RUSH are diagrammed in Fig. 6A. We created the ER-hooked version of both Q1-GFP and HA-E1-dsR and expressed them in COS-7 cells. Under the control conditions, they were retained in the ER by binding of a streptavidin binding peptide (SBP) engineered into their C-termini to a streptavidin core domain (SCD) engineered into an ER resident protein coexpressed in the same cell by the bi-cistronic RUSH plasmid. Adding membrane permeable biotin to the culture medium released Q1-GFP and HA-E1-dsR from the ER-hook, allowing them to traffic down their forward paths.

Pilot experiments showed that after biotin application, originally ER-hooked HA-E1-dsR rapidly entered a vesicular compartment while ER-hooked Q1-GFP largely stayed in the ER. To examine the nature of their trafficking paths, we expressed them separately. ER-hooked HA-E1-dsR was coexpressed with ER-hooked vesicular stomatitis virus protein G (VSVG, fused with GFP). VSVG served as a reporter for constitutive forward trafficking through the conventional secretory path (Lippincott-Schwartz *et al.*, 2000). Fig. 6B shows that before biotin application, both HA-E1-dsR and VSVG-GFP were retained in the ER. After biotin application, both exited the ER in vesicles and clustered to the

Golgi zone (30 - 60 min). By 120 min, both disappeared from the vesicular and Golgi compartments, and were present in the cell membrane.

Fig. 6C depicts a COS-7 cell coexpressing HA-E1-dsR, mCFP-tagged SEC31A (component of COPII coat, a marker of ER exit sites) and GFP-tagged ERGIC-53 (a marker of ER to Golgi intermediate compartment). The cell had been incubated in brefeldin A (BFA) to prevent proteins' ER exit (Klausner *et al.*, 1992). After BFA washout, the restriction on ER exit was lifted. We observed HA-E1-dsR vesicles appearing from ER bundles. These HA-E1-dsR vesicles partially overlapped with mCFP-SEC31A (signifying ER exit), and GFP-ERGIC-53 (signifying trafficking from ER to the Golgi). Together data presented in Fig. 6B and 6C indicate that HA-E1-dsR trafficked through the conventional secretory path, from ER through Golgi to PM, in a constitutive manner.

ER-hooked Q1-GFP was coexpressed with dsRed-ER, an ER marker (Fig. 6D). Before and up to 120 min after biotin application, the Q1-GFP distribution pattern overlapped with that of dsRed-ER, indicating that most of the Q1-GFP stayed in the ER long after it was released from the ER-hook. However, high-resolution imaging using structured illumination microscopy (SIM) revealed small submicron Q1-GFP vesicles outside the ER tubules after 45-60 min incubation with biotin (Fig. 7A). Similar findings were obtained with regular Q1-GFP (not ER-hooked) coexpressed with dsRed-ER (data not shown). To better understand the nature of these submicron Q1-GFP vesicles, we used 4D imaging (z-stack plus time lapse) to follow Q1-GFP movements inside and outside the ER. This was done using Zeiss 880 in the fast Airyscan mode, which provided the sensitivity and image quality required for detecting dynamic events of submicron objects. In the example shown in Fig. 7B, a COS-7 cell expressing Q1-GFP was imaged through seven z planes at 190 nm steps (diagrammed in panel 'a'). Time lapse was recorded with 177.2 ms between time points. Panel 'b' shows a submicron Q1-GFP vesicle breaking off from an ER bundle at time point 2 at z plane 7. At time point 3, it disappeared at z plane 7 and was not detected at z plane 6. This suggests that it moved out of the focus in the upward direction. Since z plane 7 was close to the top surface of the cell, this vesicle may have fused with the top cell membrane and the Q1-GFP was dissipated into the surface membrane.

Panel 'c' of Fig. 7B compares views of the bottom surface (z plane 2) and cell interior (z plane 6) between the first and 10th time points (1772 ms apart). There were small Q1-GFP vesicles close to the bottom surface. They were extremely dynamic so that most of the vesicles seen at the first time point did not overlap with vesicles seen at 10th time points (green and red vesicles, but rarely yellow vesicles, in the merge view). On the other hand, the ER bundles seen in z plane 6 were much more stable, so that the ER mesh seen at the first and 10th time points largely overlapped (yellow ER bundles in the merge view). Similar findings were obtained in 8 cells from two independent experiments. These Q1-GFP vesicles outside the ER tubules may represent transport vehicles exiting ER en route to the cell surface by an unconventional secretory path (Nickel & Seedorf, 2008). A direct ER to PM transport of Q1-GFP is consistent with our observations that coexpressing junctophilin-2 (JPH2, an ER-PM tether protein) with KCNQ1 in COS-7 cells increased cell surface KCNQ1 protein level (Jiang *et al.*, 2016), accompanied by an enlargement of ER-PM junctions (Jiang *et al.*, 2019).

KCNQ1 and KCNE1 assemble preferentially on the cell surface

Experiments presented above showed that in adult ventricular myocytes I_{Ks} channels, as well as cell surface KCNQ1 and KCNE1, are localized on the surface sarcolemma. Importantly, although cytoplasmic KCNQ1 and KCNE1 partially overlapped in transverse striations along the z-lines, the I_{Ks} channels did not manifest any transverse striation pattern. This distinction indicates that cytoplasmic KCNQ1 and KCNE1 did not assemble into I_{Ks} channels despite their spatial proximity. Furthermore, RUSH experiments showed that KCNQ1 and KCNE1 trafficked by separate routes from ER to the cell surface, confirming our previous indirect observations based on Q1-GFP and E1-dsR distribution in

canine ventricular myocytes (Jiang *et al.*, 2017). Do KCNQ1 and KCNE1 assemble into I_{Ks} channels after they have reached the cell surface?

To answer this question in a quantitative manner, we used a KCNQ1/KCNE1 pair that reported I_{Ks} assembly in immunoblot experiments. Previously we showed that cells expressing Q1-Q147C/E1-G40C had wild-type like I_{Ks} current under reducing conditions (DTT treatment, disrupting disulfide bonds). However, under non-reducing conditions (no DTT pretreatment), the two engineered Cys side chains could form a disulfide bond, locking the I_{Ks} channel in the open state (Wang *et al.*, 2011). To allow disulfide bond formation, C_{β} atoms of two Cys side chains need to come very close to each other, ≤ 0.46 nm apart (Careaga & Falke, 1992). This means that disulfide-bond between Q1-Q147C and E1-G40C (abbreviated as 'Q1-S-S-E1') occurred in the open state of a fully assembled I_{Ks} channel (Wang *et al.*, 2011). The degree of Q1-S-S-E1 formation can be readily quantified by non-reducing SDS-PAGE: Q1-S-S-E1 migrated as an 80 kDa band, different from the Q1 and E1 bands (60 and 20 kDa, respectively). To test whether Q1-Q147C/E1-G40C assembly preferentially occurred in the cytoplasm vs on the cell surface, we used BFA to block protein exit to the cell surface. Fig. 8A depicts two scenarios. If Q1-Q147C/E1-G40C assembly preferentially occurred in the cytoplasm, BFA incubation would not reduce, or even increase, Q1-S-S-E1 formation. If Q1-Q147C/E1-G40C assembly preferentially occurred on the cell surface, BFA incubation would reduce Q1-S-S-E1 formation.

The effectiveness of BFA incubation in preventing proteins from reaching the cell surface was confirmed by quantifying cell surface proteins with biotinylation followed by neutravidin pull-down (representative immunoblot by reducing SDS-PAGE shown in Fig. 8B, and densitometry data summarized in the lower panel of Fig. 8D). We then quantified Q1-S-S-E1 formation in cells cultured under the control conditions vs in the presence of BFA. The immunoblot image in Fig. 8C shows that control WCL run on non-reducing SDS-PAGE had two bands at 80 and 60 kDa. Pretreatment of WCL with DTT before loading collapsed the 80 kDa band into the 60 kDa band, confirming the nature of the 80 kDa band as Q1-S-S-E1. WCL from BFA-treated cells had much lower 80 kDa band intensity than that of the control WCL, and DTT pretreatment had the same effect. We used the ratio of 80 kDa to 60 kDa band intensities as a readout of Q1-S-S-E1 formation normalized by the Q1 expression level. Densitometry data are summarized in the upper panel of Fig. 8D: BFA incubation caused a 50% reduction in Q1-S-S-E1 formation. This result supports the scenario of preferential Q1-Q147C/E1-G40C assembly on the cell surface.

KCNQ1 and KCNE1 are closer to each other on the cell surface than in cytoplasm

To allow KCNQ1/KCNE1 assembly, the two must come close to each other on the cell surface. To test whether this is the case, we compared spatial proximity between Q1-GFP and HA-E1-dsR on the cell surface vs their cytoplasmic counterparts. Cell surface Q1-GFP and HA-E1-dsR were detected by incubating live COS-7 cells with Q1 ext rabbit Ab and HA mouse Ab, followed by Alexa647 goat anti-rabbit and Alexa405 goat anti-mouse Abs. Cytoplasmic Q1-GFP and HA-E1-dsR were detected by their fluorescent protein tags (Fig. 9A diagram). High density confocal images were acquired in z-stacks: xy pixel dimension 40 nm, z-steps 150 nm (a representative example shown in Fig. 9B). The raw images were deconvoluted, corrected for chromatic aberrations, and segmented. The segmented images (example shown in Fig. 9C) allowed us to discern distinct fluorescence foci, i.e. clusters of fluorescently labeled proteins, and calculated the nearest neighbor distances between them. Fig. 9D depicts the distribution of distances between nearest Q1-GFP neighbors to HA-E1-dsR on the cell surface and in cytoplasm. The median distances are 0.44 and 1.76 μ m, respectively, indicating that on average cell surface Q1-GFP and HA-E1-dsR were closer to each other than cytoplasmic counterparts.

The wider separation between Q1-GFP and HA-E1-dsR in the cytoplasmic compartment is consistent with their separate trafficking routes. How did they come close to each other when they had reached the cell surface? There are two possible mechanisms. First, they might preferentially cluster to

the lipid raft domains of surface membrane, as has been shown for their native counterparts in guinea pig ventricular myocytes (Nakamura *et al.*, 2007). Second, cell surface KCNQ1 and KCNE1 may concentrate in PIP₂-enriched regions, due to electrostatic attraction between negatively charged PIP₂ headgroups and the high positive charge densities in the juxtamembrane cytoplasmic domains of KCNQ1 and KCNE1 (Li *et al.*, 2011; Zaydman & Cui, 2014).

Search for KCNQ1 and KCNE1 interactors using affinity purification and liquid chromatography/tandem mass spectrometry (LC/MS-MS)

During their separate journeys from ER to the plasma membrane, Q1-GFP and HA-E1-dsR may interact with different proteins (interactors). During their clustering to the same microdomains on cell surface and eventual assembly into functional I_{Ks} channels, Q1-GFP and HA-E1-dsR may interact with the same set of protein interactors. To search for their interactors in a global and unbiased manner, we applied LC/MS-MS to affinity-purified Q1-GFP and HA-E1-dsR, and checked what other proteins were co-purified as putative interactors. To take advantage of the much more complete human protein database than other species, we used human embryonic kidney (HEK293) cells as the expression system. HEK293 cells were cotransfected with Q1-GFP and HA-E1-dsR, or untransfected (the latter served as negative control, labeled as '-cDNA' in Fig. 10A). Whole cell lysates (WCLs) were made under mild detergent conditions (1% Triton X-100) to preserve noncovalent protein-protein associations. Each WCL was divided into three equal aliquots, used for immunoprecipitation with dsR rabbit Ab, GFP rabbit Ab, and GFP goat Ab, respectively. To check the quality of the immunoprecipitates (IPs) and whether non-covalent protein-protein associations were preserved, we fractionated WCLs, negative and positive IPs ([-] and [+] IPs, from untransfected and transfected cells respectively) by SDS-PAGE. After the proteins were transferred to a PVDF membrane, the membrane was cut between 75 and 50 kDa size marker bands. The upper portion was probed with GFP goat Ab (WCLs and IPs with rabbit Abs) or GFP rabbit Ab (IPs with GFP goat Ab). The lower portion was probed with HA mouse Ab (Fig. 10A). The immunoblots show that dsR Ab immunoprecipitated HA-E1-dsR effectively. Furthermore, the presence of Q1-GFP in [+] IPs with dsR Ab, i.e. Q1-GFP/HA-E1-dsR coimmunoprecipitation, confirmed that non-covalent protein-protein association was preserved. Likewise, GFP rabbit Ab and GFP goat Ab were able to immunoprecipitate Q1-GFP, although differing in their preference for monomer vs dimer Q1-GFP. We also detected HA-E1-dsR in [+] IPs by both GFP Abs, confirming again the preservation of non-covalent protein-protein association. GFP goat Ab detected a band in WCL from untransfected cells and [-] IP with GFP rabbit Ab similar in size to Q1-GFP monomer (marked by '?' in Fig. 10A). Similar findings were obtained in a pilot experiment conducted in the same manner as described in Fig. 10A. Therefore, this band was a consistent finding, although its nature is unclear.

The [+] and [-] IP samples were subject to LC/MS-MS analysis. Detailed description of the LC/MS-MS procedures is provided in the *Methods* section. Search of mass spectrometry data against the Uniprot human protein database produced nine protein lists, that were combined in the following manner before analysis: (1) protein lists from the four [+] IPs with GFP Abs were combined as [+] IP of Q1-GFP, (2) protein lists from the two [-] IPs with GFP Abs were combined as [-] IP of Q1-GFP, and (3) protein lists from the two [+] IPs with dsR Ab were combined as [+] IP of HA-E1-dsR. We used two filters to retain high-confidence proteins from these lists. First, we retained those proteins identified in the [+] IPs with at least two unique peptide-spectrum matches ($\Sigma\text{PSM} \geq 2$). This filter eliminated potential artifacts due to opportunistic peptide matches. Second, from the above protein lists we retained those absent in the [-] IPs, and those detected in the [-] IPs but at a lower level than in the [+] IPs (ΣPSM ratio of [+] IP:[-] IP ≥ 2). In total, we found 109 proteins each in Q1-GFP and HA-E1-dsR immunoprecipitates. These proteins, along with their ΣPSM data, are listed in Tables 1 and 2 of the Appendix.

As a test of the validity of proteomics data, we focused on a novel putative KCNQ1 interactor: microtubule plus-end binding protein 1 (EB1). EB1 was found in Q1-GFP [+] IP, but not HA-E1-dsR

[+] IP in LC/MS-MS experiments. Fig. 10B shows that an EB1 dimer band was highly abundant in the [+] IP by GFP rabbit Ab but very dim in the [+] IP by dsR rabbit Ab (ratio of band intensity 10:1). This is consistent with the proteomics data. The functional implication of Q1-GFP interaction with EB1 dimer is not clear. It has been shown that dimerization of EB1 is phosphorylation-dependent, and can influence EB1 binding to microtubules (Chen *et al.*, 2014).

EB1 guides and facilitates KCNQ1 to reach cell surface

We further tested whether native EB1 preferentially bound Q1-GFP, but not HA-E1-dsR, in cardiac myocytes. Rat ventricular myocytes were transduced with Q1-GFP and HA-E1-dsR, cultured for 36 hr before lysis with 1% Triton X-100. The whole cell lysate was divided into three aliquots and subject to immunoprecipitation with GFP rabbit Ab, HA mouse Ab and EB1 rat Ab, respectively. WCL, negative control ([-] IP, WCL incubated with protein A/G beads without Abs), and [+] IP samples were fractionated by SDS-PAGE, and probed with Abs listed on the left side of Fig. 11Aa. We detected reciprocal coimmunoprecipitation between Q-GFP and native EB1 dimer. While the HA-E1-dsR was co-immunoprecipitated with Q1-GFP reciprocally, there was no EB1 band in the HA-E1-dsR [+] IP. The same results were obtained in two independent experiments, confirming that EB1 interacted with Q1-GFP but not HA-E1-dsR expressed in cardiac myocytes.

Fig. 11Ab shows that in a rat ventricular myocyte transduced with Q1-GFP, cell surface Q1 (detected by Q1 ext Ab as described for Fig. 5) but not cytoplasmic Q1-GFP were highly colocalized with native EB1. In the cell center view, surface Q1 and cytoplasmic EB1 overlapped at the cell ends (intercalated disc, ICD, region). EB1 clustering to ICD is consistent with its established role of guiding connexin 43 to this area of myocytes (Shaw *et al.*, 2007). In the cell surface view, both surface Q1 and subsarcolemmal EB1 were in distinct puncta overlapping with each other. Similar observations were obtained from 6 myocytes from two independent experiments examined in the same manner. These observations suggest that EB1 may guide Q1-GFP trafficking along microtubules toward the plus ends at myocyte periphery, thus helping deliver Q1-GFP to the cell surface. To test whether this was the case, we compared the distribution pattern of Q1-GFP expressed alone or coexpressed with EB1-dTomato in COS-7 cells (Fig. 11B). Q1-GFP expressed alone was in the ER tubules in all cells examined. In the presence of EB1-dTomato, eight out of ten cells had Q1-GFP on the cell surface and in cytoplasmic EB1-positive structures. Together Fig. 11 shows that EB1 preferentially binds Q1-GFP and facilitates its delivery to the cell surface.

DISCUSSION

Proteomics data provide new insights into KCNQ1 and KCNE1 trafficking in cells

We divided the proteins found in Q1-GFP and HA-E1-dsR immunoprecipitates into three groups: uniquely in Q1-GFP immunoprecipitate (41), uniquely in HA-E1-dsR immunoprecipitate (41), and shared between the two (68, Venn diagram in Fig. 12A). We then manually curated these three groups of proteins, and selected those known to be involved in protein trafficking and distribution. These proteins are tabulated in Fig. 12B, categorized by their cellular compartments or molecular functions (first column). Based on Fig. 12B, in conjunction with information from our current and previous experimental findings (Wang *et al.*, 2013; Jiang *et al.*, 2017), we present a synthetic view of how KCNQ1 and KCNE1 traffic and assemble in cells (Fig. 12C).

The following are shared interactors between Q1-GFP and HA-E1-dsR, that provide clues as to how the two travel and distribute in cells:

1. Both Q1-GFP and HA-E1-dsR interacted with of ER proteins (calnexin, Erlin-2, and calreticulin) and chaperones (heat-shock proteins and isoforms of T-complex 1), reflecting their translation in the rough ER, and dependence on the chaperones for proper folding.

2. Both Q1-GFP and HA-E1-dsR interacted with α and β tubulins, consistent with cargo vesicles traveling on microtubule (MT) tracks.
3. Both Q1-GFP and HA-E1-dsR interacted with actin isoforms (α , β and β 2-like) and conventional, non-muscle myosin-9 and myosin-10. These myosin motors move vesicles along actin filaments toward the barbed ends at the plasma membrane (Chantler *et al.*, 2010), suggesting that KCNQ1- and KCNE1-containing cargo vesicles traffic on cortical actin filaments before fusion with the plasma membrane.
4. Both Q1-GFP and HA-E1-dsR interacted with actin-binding proteins: α -actinin-4 and filamin-A. HA-E1-dsR also interacted with intermediate filament, vimentin. These interactors may anchor KCNQ1 and KCNE1 on the cell surface by cortical cytoskeleton.
5. Both Q1-GFP and HA-E1-dsR interacted with flotillin-1, a lipid-raft resident protein. This is consistent with clustering of native KCNQ1 and KCNE1 to lipid rafts in guinea pig heart (Nakamura *et al.*, 2007).
6. Both Q1-GFP and HA-E1-dsR interacted with Rab5c. HA-E1-dsR also interacted with Rab10. These small GTPases mediate endocytosis of plasma membrane proteins.
7. Both Q1-GFP and HA-E1-dsR interacted with 14-3-3 proteins. 14-3-3 proteins coordinate the organization of microtubules and actin filaments (Shikano *et al.*, 2006). The functional implications of 14-3-3 interaction with KCNQ1 and KCNE1 require future investigation.
8. Both Q1-GFP and HA-E1-dsR interacted with components of desmosomal junction. These interactors may explain why surface KCNQ1 and KCNE1 cluster to the intercalated disc region of cardiac myocytes (Figs. 1A and 1C) (Balse *et al.*, 2012).

Interactors unique to Q1-GFP or HA-E1-dsR also provide clues as to how the two travel separately in cells:

1. HA-E1-dsR uniquely bound ER-to-Golgi SNARE of 24 kDa (also called Sec22B). This, in conjunction with our observations that after exiting the ER, HA-E1-dsR entered a vesicular compartment overlapping with Sec31A (COPII component) and ERGIC-53 (ER-to-Golgi intermediate compartment), supports the view that HA-E1-dsR trafficked by the conventional secretory path from ER to Golgi and then cell surface (Lippincott-Schwartz *et al.*, 2000). Importantly, there was no protein involved in ER to Golgi transport found in Q1-GFP immunoprecipitate. This is consistent with the notion that Q1-GFP trafficked from ER to plasma membrane bypassing the Golgi.
2. Q1-GFP, but not HA-E1-dsR, interacted with EB1 and kinesin-1. EB1 mediates tip attachment complex (TAC) formation between the tips of ER tubules and the plus-ends of MT, so that the ER tubules grow in concert with the MT plus-ends toward cell periphery (Friedman & Voeltz, 2011). The motor protein, kinesin-1, pulls ER tubules out of the ER cisternae and move them along MT tracks toward cell periphery, creating the so-called ER sliding events (Friedman & Voeltz, 2011). We often observed both TAC and ER sliding events in live cell imaging of Q1-GFP (data not shown), signaling Q1-GFP in ER tubules moving toward the cell periphery.
3. Q1-GFP, but not HA-E1-dsR, interacted with vinculin and talin-1. These two proteins, together with integrins, form a macromolecular complex at cell-extracellular matrix (ECM) junctions (Henderson *et al.*, 2017). These interactors may explain why cell surface KCNQ1 clusters to surface sarcolemma (facing ECM) but not t-tubules in cardiac myocytes.
4. Q1-GFP interacted with Rap1b-like protein. This may be related to the interaction of Q1-GFP with vinculin and talin-1, because Rap1 is involved in integrin activation (Henderson *et al.*, 2017).

Delayed KCNQ1/KCNE1 assembly in the surface sarcolemma is an integral part of I_{Ks} function: segregated under basal conditions and mobilized in response to β -adrenergic stimulation

Our data showed that the transverse striation pattern seen in immunofluorescence signals of native KCNQ1 in ventricular myocytes from canine (Jiang *et al.*, 2017), guinea pig (Wang *et al.*, 2013) and rat (Rasmussen *et al.*, 2003; Oliveras *et al.*, 2020) hearts represents KCNQ1 in a cytoplasmic compartment, most likely the junctional SR. On the other hand, native KCNE1 in ventricular myocytes from canine and guinea pig hearts is mainly on the surface sarcolemma (Wang *et al.*, 2013; Jiang *et al.*, 2017). Immunofluorescence signals of native KCNE1 in rat ventricular myocytes do have a transverse striation component (Wu *et al.*, 2006; Oliveras *et al.*, 2020). This may represent a cytoplasmic pool of KCNE1 being directed to the jSR compartment after assembly with KCNQ1 (Oliveras *et al.*, 2020).

Lone KCNE1 on the surface sarcolemma does not have I_{Ks} function. It is in a standby mode, waiting for KCNQ1 to exit the jSR compartment. KCNQ1-containing vesicles may travel along microtubules, guided by EB1, to the sarcolemma where KCNQ1 associates with KCNE1 to form I_{Ks} channels. Indeed, KCNQ1 mobilization along microtubules is required for the 'amplitude response' of I_{Ks} channels to β -adrenergic stimulation (Nicolas *et al.*, 2008). This was revealed by the observations that microtubule depolymerization by colchicine prevents the amplitude response of I_{Ks} to β -adrenergic stimulation, despite intact gating response and intact PKA-mediated phosphorylation of both S27 in KCNQ1 and S43 in yotiao (Nicolas *et al.*, 2008). Unconventional trafficking path of KCNQ1, directly from jSR to the sarcolemma, expedites the formation of new I_{Ks} channels critical for a timely response to β -adrenergic stimulation.

REFERENCES

- Balse E, Steele DF, Abriel H, Coulombe A, Fedida D & Hatem SN. (2012). Dynamic of ion channel expression at the plasma membrane of cardiomyocytes. *Physiological Review* **92**, 1317-1358.
- Banyasz T, Jian Z, Horvath B, Khabbaz S, Izu LT & Chen-Izu Y. (2014). Beta-adrenergic stimulation reverses the IKr-IKs dominant pattern during cardiac action potential. *Pflugers Arch* **466**, 2067-2076.
- Bas T, Gao GY, Lvov A, Chandrasekhar KD, Gilmore R & Kobertz WR. (2011). Post-translational N-glycosylation of type I transmembrane KCNE1 peptides. Implications for membrane protein biogenesis and disease. *J Biol Chem* **286**, 28150-28159.
- Boncompain G, Divoux S, Gareil N, de Forges H, Lescure A, Latreche L, Mercanti V, Jollivet F, Raposo G & Perez F. (2012). Synchronization of secretory protein traffic in populations of cells. *Nature Methods* **9**, 493-498.
- Borggreffe M, Wolpert C, Antzelevitch C, Veltmann C, Giustetto C, Gaita F & Schimpf R. (2005). Short QT syndrome genotype-phenotype correlations. *J Electrocardiology* **38**, 75-80.
- Caballero R, de la Fuente MG, Gomez R, Barana A, Amoros I, Dolz-Gaiton P, Osuna L, Almendral J, Atienza F, Fernandez-Aviles F, Pita A, Rodriguez-Roda J, Pinto A, Tamargo J & Delpon E. (2010). In humans, chronic atrial fibrillation decreases the transient outward current and ultrarapid component of the delayed rectifier current differentially on each atria and increases the slow component of the delayed rectifier current in both. *J Am Coll Cardiol* **55**, 2346-2354.
- Careaga CL & Falke JJ. (1992). Thermal motions of surface α -helices in the D-galactose chemosensory receptor. Detection by disulfide trapping. *Journal of Molecular Biology* **226**, 1219-1235.
- Chandrasekhar KD, Bas T & Kobertz WR. (2006). KCNE1 subunits require co-assembly with K^+ channels for efficient trafficking and cell surface expression. *J Biol Chem* **281**, 40015-40023.
- Chandrasekhar KD, Lvov A, Terrenoire C, Gao GY, Kass RS & Kobertz WR. (2011). O-glycosylation of the cardiac I_{Ks} complex. *J Physiol* **589**, 3721-3730.

- Chantler PD, Wylie SR, Wheeler-Jones CP & McGonnell IM. (2010). Conventional myosin-unconventional functions. *Biophysical Review* **2**, 67-82.
- Chen J, Luo Y, Li L, Ran J, Wang X, Gao S, Liu M, Li D, Shui W & Zhou J. (2014). Phosphoregulation of the dimerization and functions of end-binding protein 1. *Protein Cell* **5**, 795-799.
- David J-P, Andersen MN, Olesen S-P, Rasmussen HB & Schmitt N. (2013). Trafficking of the I_{Ks} -complex in MDCK cells: site of subunit assembly and determinants of polarized localization. *Traffic* **14**, 399-411.
- Friedman JR & Voeltz GK. (2011). The ER in 3D: a multifunctional dynamic membrane network. *Trends in Cell Biology* **21**, 709-717.
- Henderson CA, Gomez CG, Novak SM, Mi-Mi L & Gregorio CC. (2017). Overview of the muscle cytoskeleton. *Comprehensive Physiology* **7**, 891-944.
- Jiang M, Hu J, White FKH, Williamson J, Klymchenko AS, Murthy A, Workman SW & Tseng G-N. (2019). S-palmitoylation of junctophilin-2 is critical for its role in tethering the sarcoplasmic reticulum to the plasma membrane. *J Biol Chem* **294**, 13487-13501.
- Jiang M, Wang Y-H & Tseng G-N. (2017). Adult ventricular myocytes segregate KCNQ1 and KCNE1 to keep the I_{Ks} amplitude in check until when larger I_{Ks} is needed. *Circ Arrhythm Electrophysiol* **10**, e005084.
- Jiang M, Zhang M, Howren M, Wang YH, Tan A, Balijepalli RC, Huizar JF & Tseng G-N. (2016). JPH-2 interacts with Ca_i -handling proteins and ion channels in dyads: contribution to premature ventricular contraction-induced cardiomyopathy. *Heart Rhythm* **13**, 743-752.
- Jost N, Virag L, Bitay M, Takacs J, Lengyel C, Biliczki P, Nagy Z, Bogats G, Lathrop DA, Papp JG & Varro A. (2005). Restricting excessive cardiac action potential and QT prolongation. A vital role for I_{Ks} in human ventricular muscle. *Circulation* **112**, 1392-1399.
- Klausner RD, Donaldson JG & Lippincott-Schwartz J. (1992). Brefeldin A: insights into the control of membrane traffic and organelle structure. *J Cell Biol* **116**, 1071-1080.
- Krumerman A, Gao X-H, Bian J-S, Melman YF, Kagan A & McDonald TV. (2004). An LQT mutant minK alters KvLQT1 trafficking. *Am J Physiol* **286**, C1453-C1463.
- Li Y, Hof T, Baldwin TA, Chen L, Kass RK & Dessauer CW. (2019). Regulation of I_{Ks} potassium current by isoproterenol in adult cardiomyocytes requires type 9 adenylate cyclase. *Cells* **8**, 981.
- Li Y, Zaydman MA, Wu D, Shi J, Guan M, Virgin-Downey B & Cui J. (2011). KCNE1 enhances phosphatidylinositol 4,5-bisphosphate (PIP₂) sensitivity of I_{Ks} to modulate channel activity. *PNAS* **108**, 9095-9100.
- Lippincott-Schwartz J, Roberts TH & Hirschberg K. (2000). Secretory protein trafficking and organelle dynamics in living cells. *Ann Rev Cell Dev Biol* **16**, 557-589.
- Marx SO, Reiken S, Hisamutsu Y, Jayaraman T, Burkhoff D, Rosemblyt N & Marks AR. (2000). PKA phosphorylation dissociates FKBP12.6 from the calcium release channel (ryanodine receptor): defective regulation in failing hearts. *Cell* **101**, 365-376.
- Mashanov GI, Nobels M, Harmer SC, Molloy JE & Tinker A. (2010). Direct observation of individual KCNQ1 potassium channels reveals their distinctive diffusive behavior. *J Biol Chem* **285**, 3664-3675.

- Nakamura H, Kurokawa J, Bai C-X, Asada K, Xu J, Oren RV, Zhu ZI, Clancy CE, Isobe M & Furukawa T. (2007). Progesterone regulates cardiac repolarization through a nongenomic pathway. An in vitro patch-clamp and computational modeling study. *Circulation* **116**, 2913-2922.
- Nickel W & Seedorf M. (2008). Unconventional Mechanisms of Protein Transport to the Cell Surface of Eukaryotic Cells. *Annu Rev Cell Dev Biol* **24**, 287-308.
- Nicolas CS, Park K-H, Harchi AE, Camonis J, Kass RS, Escande D, Merot J, Loussouarn G, Le Bouffant F & Baro I. (2008). I_{Ks} response to protein kinase A-dependent KCNQ1 phosphorylation requires direct interaction with microtubules. *Cardiovas Res* **79**, 427-435.
- Oliveras A, Serrano-Novillo C, Moreno C, de la Cruz A, Valenzuela C, Soeller C, Comes N & Felipe A. (2020). The unconventional biogenesis of Kv7.1-KCNE1 complexes. *Science Advances* **6**, eaay4472.
- Rasmussen HB, Moller M, Knaus H-G, Jensen BS, Olesen S-P & Jorgensen NK. (2003). Subcellular localization of the delayed rectifier K^+ channels KCNQ1 and ERG1 in the rat heart. *Am J Physiol* **286**, H1300-H1309.
- Sanguinetti MC, Curran ME, Zou A, Shen J, Spector PS, Atkinson DL & Keating MT. (1996). Coassembly of KvLQT1 and minK (IsK) proteins to form cardiac I_{Ks} potassium channel. *Nature* **384**, 80-83.
- Sarkar AX & Sobie EA. (2016). Quantification of repolarization reserve to understand interpatient variability in the response to proarrhythmic drugs: A computational analysis. *Heart Rhythm* **8**, 1749-1755.
- Shaw RM, Fay AJ, Puthenveedu MA, von Zastrow M, Jan Y-N & Jan LY. (2007). Microtubule plus-end-tracking proteins target gap junctions directly from the cell interior to adherens junctions. *Cell* **128**, 547-560.
- Shikano S, Coblitz B, Wu M & Li M. (2006). 14-3-3 proteins: regulation of endoplasmic reticulum localization and surface expression of membrane proteins. *Trends in Cell Biology* **16**, 370-375.
- Soderberg O, Leuchowius K-J, Gullberg M, Jarvius M, Weibrecht I, Larsson L-G & Landegren U. (2008). Characterizing proteins and their interactions in cells and tissues using the in situ proximity ligation. *Methods* **45**, 227-232.
- Splawski I, Shen J, Timothy KW, Lehmann MH, Priori SG, Robinson JL, Moss AJ, Schwartz PJ, Towbin JA, Vincent GM & Keating MT. (2000). Spectrum of mutations in long-QT syndrome genes *KvLQT1*, *HERG*, *SCN5A*, *KCNE1*, and *KCNE2*. *Circulation* **102**, 1178-1185.
- Sun J & MacKinnon R. (2020). Structural basis of human KCNQ1 modulation and gating. *Cell* **180**, 340-347.
- Vanoye CG, Welch RC, Tian C, Sanders CR & George ALJ. (2010). KCNQ1/KCNE1 assembly, co-translation not required. *Channels (Austin)* **4**, 108-114.
- Wang Y-H, Jiang M, Xu X-L, Hsu K-L, Zhang M & Tseng G-N. (2011). Gating-related molecular motions in the extracellular domain of the I_{Ks} channel: implications for I_{Ks} channelopathy. *J Memb Biol* **239**, 137-156.
- Wang Y-H, Zankov DP, Jiang M, Zhang M, Henderson SC & Tseng G-N. (2013). $[Ca]_i$ elevation and oxidative stress induce KCNQ1 translocation from cytosol to cell surface and increase I_{Ks} in cardiac myocytes. *J Biol Chem* **288**, 35358-35371.

Wu D-M, Jiang M, Zhang M, Liu X-S, Korolkova YV & Tseng G-N. (2006). KCNE2 is colocalized with KCNQ1 and KCNE1 in cardiac myocytes and may function as a negative modulator of I_{Ks} current amplitude in the heart. *Heart Rhythm* **3**, 1469-1480.

Xu Y, Wang YH, Meng X-Y, Zhang M, Jiang M, Zhang H-X, Cui M & Tseng G-N. (2013). Building KCNQ1/KCNE1 docking models and probing their interactions by molecular dynamics simulations. *Biophysical Journal* **105**, 2461-2473.

Zaydman MA & Cui J. (2014). PIP2 regulation of KCNQ channels: biophysical and molecular mechanisms for lipid modulation of voltage-dependent gating. *Frontiers in Physiology* **5**, article 195.

CONFLICT OF INTEREST None.

ACKNOWLEDGEMENTS

Confocal microscopy was performed at the Virginia Commonwealth University – Department of Neurobiology & Anatomy Microscopy Facility, supported in part by NIH-NINDS Center Core Grant 5P30NS047463.

FUNDING

This study was supported by NIH/NHLBI (HL128610, HL96962, and HL94450).

FIGURE LEGENDS

Fig. 1 Fluorescent protein- and epitope-tagged KCNQ1 and KCNE1 retain their distribution patterns in cardiac myocytes and normal I_{Ks} channel function. (A) Confocal images of Q1-GFP and HA-E1-dsR expressed in a rat ventricular myocyte. Z-stack images were obtained (diagram on top), and shown are XY plane view at the central z-plane and a selected XZ plane view (locations noted by the white dashed lines in XY plane view). Overlap between Q1-GFP and HA-E1-dsR in the XZ plane view is marked by asterisks in the 'merge' panel. (B) Currents recorded from COS-7 cells transfected with Q1-GFP and HA-E1-dsR. Cells were superfused with normal Tyrode's solution at 24°C, and whole cell currents were recorded with the standard K-aspartate pipette solution (see Methods). *Top*: current traces elicited by the voltage clamp protocol diagrammed in the inset. *Bottom*: Boltzmann fit to the voltage-dependence of channel activation, estimated by the relationship between the test pulse voltages (V_t) and the peak tail current amplitudes (I_{peak}), degree of activation = $(I_{max}/I_{peak})/(1+\exp((V_{0.5}-V_t)/k))$, where I_{max} , $V_{0.5}$ and k are the estimated maximal peak tail current amplitude of the cell, half-maximum activation voltage and slope factor, respectively. The parameter values are listed in the inset. (C) Confocal images of immunofluorescence of native KCNQ1 and KCNE1 in a guinea ventricular myocyte. KCNQ1 and KCNE1 were labeled with goat and mouse primary antibodies, followed by Alexa-488 donkey anti-goat and Alexa-568 donkey anti-mouse secondary Abs. The format of this panel is the same as that of panel (A). (D) Native I_{Ks} recorded from guinea pig ventricular myocytes. Myocytes were superfused with a Na- and Ca-free Tyrode's solution (replaced by equimolar choline and Mg) to avoid I_{Ks} contamination by Na and Ca channel currents, at 33°C. Whole cell currents were recorded with the standard K-aspartate pipette solution. The format of this panel is the same as that of (B).

Fig. 2 Localize KCNQ1/KCNE1 assembly in cardiac myocytes by *in situ* proximity ligation assay (PLA). Rat ventricular myocytes transduced with Q1-GFP and HA-E1-dsR were cultured for 24 hr before experiments. (A) Diagram of PLA procedure. Primary antibodies (1st Abs) were GFP mouse Ab and dsRed rabbit Ab, binding to the FP tags in the cytoplasmic compartment. At sites where the 1st Abs were ≤ 40 nm apart, binding of nucleotide-conjugated PLA probes to the 1st Abs allowed nucleotide

ligation and amplification. During the latter reaction, far red fluorophore was incorporated to mark these sites. Not shown in the diagram: after PLA procedure, myocytes were incubated with Alexa488 goat anti-mouse and Alexa568 goat anti-rabbit Abs to label total Q1-GFP and HA-E1-dsR. **(B)** Representative images of Z-projection of maximum signals of Q1-GFP, HA-E1-dsR and PLA from a myocyte. A total of 29 Z-slices was acquired, and 20 Z-slices (excluding the bottom 6 and the top 3 slices to avoid interference by cell surface PLA signals) were used to create the Z-projections (diagrammed on top). The PLA signal is pseudo colored white. **(C)** Quantification of Q1-GFP, HA-E1-dsR and PLA signals in cell periphery. The % of signals in an area of 2 μm wide within the cellular contour was determined. Shown are data points from individual myocytes (symbols, 8 myocytes from 2 animals) and mean \pm SD (bar graph). The three groups of data were subject to one-way ANOVA ($p=0.001$), followed by Tukey pairwise tests. PLA signals have higher % in cell periphery than Q1-GFP and HA-E1-dsR.

Fig. 3 Check for non-specific signals from *in situ* proximity ligation assay (PLA) used to detect KCNQ1/KCNE1 assembly. Rat ventricular myocytes were incubated for the noted numbers of hours without or with adenovirus transduction of Q1-GFP and HA-E1-dsR. The PLA procedure and incubation with Alexa conjugated secondary Abs were the same as those described for Fig. 2. Asterisks mark non-specific PLA signals in nuclei of myocytes after 36 hr culture.

Fig. 4 Check the specificity of Q1 ext Ab and HA Ab in detecting cell surface Q1-GFP and HA-E1-dsR. **(A)** In unpermeabilized COS-7 cells, Q1 ext Ab IF signals were detected in cell 1 expressing abundant Q1-GFP, but not in cell 2 not expressing Q1-GFP based on the GFP fluorescence (GFP FP). Cellular contours are marked by dotted white line (cell 1) or dashed yellow line (cell 2). **(B)** HA Ab immunofluorescence (HA Ab IF) was not detectable in control rat ventricular myocytes without or with cell membrane permeabilization. Myocyte images were shown by fluorescence of wheat germ agglutinin (WGA).

Fig. 5 Distinguish between cell surface and total KCNQ1 and KCNE1 in cardiac myocytes. Adult rat ventricular myocytes transduced with Q1-GFP and HA-E1-dsR were fixed. Myocytes labeled as '*Unpermeabilized*' were incubated with a Q1 rabbit Ab targeting aa 284 -297 in the extracellular domain of KCNQ1 (Q1 ext Ab), or HA mouse Ab (targeting HA epitope in the extracellular domain of HA-E1-dsR). This was followed by Alexa647-conjugated secondary Abs. Myocytes labeled as '*Permeabilized*' were incubated with 0.1% Triton X-100 at room temperature for 10 min to permeabilize the cell membrane. This was followed by incubation with the same primary (Q1 ext Ab and HA Ab) and secondary Abs. **(A)** Representative confocal images. Immunofluorescence (IF) signals from Q1 ext Ab and HA Ab report cell surface proteins (*Unpermeabilized*) or total proteins (*Permeabilized*), while fluorescence signals from GFP and dsRed (GFP FP and dsRed FP) report total Q1-GFP and HA-E1-dsR. White dashed lines denote where the fluorescence signal profiles in (B) were determined. **(B)** Profiles of fluorescence signals across myocyte width. Black and magenta traces represent FP and IF signals, respectively. The fluorescence profiles and cell widths were normalized to values between 0 and 1.0. Gray shading denotes where cell periphery signals in (C) were quantified. **(C)** Quantification of FP and IF signals in cell periphery of unpermeabilized myocytes. The percentage (%) of areas beneath the profile in the 0-0.2 and 0.8-1 cell width ranges was quantified for Q1-GFP and Q1-ext Ab IF (18 myocytes from 5 animals), and for HA-E1-dsR and HA Ab IF (9 myocytes from 3 animals). Shown are data points (circles) from individual myocytes and mean \pm SD (bar graph), with p values by t-test.

Fig. 6 Track KCNE1 and KCNQ1 movements after their ER exit by the 'retention using selected hook' (RUSH) strategy. (A) Diagram of RUSH procedure. Protein-of-interest (POI) was fused with a streptavidin-binding-peptide (POI-SBP) and subcloned into a bi-cistronic plasmid (with internal ribosome entry 'IRE') that had an upstream ER-resident protein (an isoform of the human invariant chain of the major histocompatibility complex, Ii, retained in the ER membrane by a double arginine motif in its cytoplasmic domain (Boncompain *et al.*, 2012)) fused with 'streptavidin core domain' (ER-hook-SCD). POI-SBP and ER-hook-SCD were translated as two independent proteins in the same cells. COS-7 cells were transfected with RUSH plasmid and cultured under the control conditions, during which the POI-SBP was retained at the ER by ER-hook-SCD. Biotin (membrane permeable) added to the culture medium would compete off POI-SBP from the ER-hook-SCD, allowing POI-SBP to exit ER and travel down its secretory path. (B) Comparison of distribution patterns of ER-hooked HA-E1-dsR and ER-hooked VSVG (vesicular stomatitis virus protein G, a reporter of the constitutive anterograde trafficking pathway, tagged with GFP) (Lippincott-Schwartz *et al.*, 2000). Shown are images of COS-7 cells coexpressing the two before and at specified time points after biotin application. *: Surface expression of HA-E1-dsR and VSVG-GFP. (C) Partial overlap among HA-E1-dsR vesicles after exiting the ER and mCFP tagged SEC31A (COPII component) and/or GFP tagged ERGIC-53 (marker of ER to Golgi intermediate component). (D) Comparison of distribution patterns of ER-hooked Q1-GFP and dsRed-ER (ER-resident protein fused with dsRed, as an ER marker). Shown are images of COS-7 cells coexpressing the two before and at specified time points after biotin application.

Fig. 7 Detect dynamic Q1-GFP vesicles outside the ER. (A) Detection of Q1-GFP-positive vesicles outside ER tubules in a COS-7 cell expressing ER-hooked Q1-GFP and dsRed-ER after 60 min incubation with 100 μ M biotin. Images were obtained with structured illumination microscopy (SIM). In the 'merge' panel, Q1-GFP was largely colocalized with dsRed-ER (yellow bundles). However, Q1-GFP vesicles of sub-micron sizes were detected outside the ER bundles, better seen in the enlarged view. (B) Live cell 4D (z-stack and time-lapse) imaging to monitor dynamic Q1-GFP vesicles. Portion of a COS-7 cell expressing Q1-GFP alone was imaged with Zeiss 880 in the fast Airyscan mode: image size 144x144 pixels, pixel dimension 90 nm, 7 z slices with 190 nm increments, and 177.2 ms per z-stack. **a:** Diagram of a cell showing z-planes 1-7 from bottom to top. **b:** Time lapse images from z planes 6 and 7 of the first 3 time points (0, 0.18 and 0.36 sec, marked). Cyan arrow points to a Q1-GFP vesicles budding off the ER seen at z plane 7 at the second time point. It disappeared from z plane 7 at the third time point but was not detected at z plane 6, suggesting that it might have fused with the cell membrane. **c:** Time lapse images from z planes 2 and 6 at first and 10th time points (pseudo-colored red and green, respectively), and their merge. At z plane 6, the ER morphology was relatively stable shown by the overlap in the 'Merge' view. On the other hand, at z plane 2 close to the bottom cell surface, Q1-GFP vesicles were dynamic so that they did not overlap between the two time points.

Fig. 8 Test preference of KCNQ1 and KCNE1 assembly inside cells or on cell surface. (A) Experimental design. COS-7 cells transfected with Q1-Q147C and E1-G40C were cultured under the control conditions or in the presence of brefeldin A (BFA, 25 μ g/ml, preventing proteins from reaching the cell surface). The two Cys side chains (147C on Q1 and 40C on E1) could come very close to each other to form a disulfide bond in the open state of a fully-assembled KCNQ1/KCNE1 channel. Therefore, the abundance of Q1-S-S-E1 reported the degree of KCNQ1/KCNE1 assembly. Two scenarios are depicted. *left:* Q1 and E1 preferentially assemble in the cytoplasm. Forcing Q1-Q147C and E1-G40C to stay inside cells by BFA would not prevent, or even encourage, Q1-S-S-E1 formation. *Right:* Q1 and E1 preferentially assemble on the cell surface. BFA would prevent Q1-S-S-E1 formation. (B) Testing the effectiveness of incubation with BFA in preventing proteins from reaching the cell surface. Cell surface proteins were biotinylated with an amine-reactive biotin derivative, and

biotinylated fraction was purified from whole cell lysate using neutravidin bead pull-down. *Top*: A representative immunoblot image of W(CL) and b(iotinylated) fraction probed by Ab targeting Q1. *Bottom*: immunoblot of a cytoplasmic protein, actin, confirming no contamination by cytoplasmic proteins in biotinylated fraction. Lower panel of (D): densitometry quantification of % cell surface Q1. Under the control conditions, Q1-Q147C reached the same level of cell surface expression as Q1-WT. Incubation with BFA markedly reduced surface level of Q1-Q147C, indicating that BFA treatment effectively prevented Q1-Q147C (and E1-G40C, by inference) from reaching the cell surface. (C) Quantification of degree of Q1-S-S-E1 formation by non-reducing SDS-PAGE. Shown is a representative immunoblot image. WCL from cells expressing Q1-Q147C and E1-G40C cultured under the control conditions or in the presence of BFA (-BFA and +BFA, respectively), without or with reducing agent pretreatment (DTT, breaking disulfide bonds) were analyzed by immunoblot with Ab targeting Q1. The 80 kDa band represented disulfide-linked Q1-Q147C/E1-G40C, confirmed by DTT treatment which collapsed the 80 kDa band into the 60 kDa band. Upper panel of (D): quantification of KCNQ1/KCNE1 assembly (80 kDa divided by 60 kDa band intensity). Incubation with BFA significantly reduced KCNQ1/KCNE1 assembly, supporting the scenario shown on right in (A). In (D), (n): # of independent experiments, T-test * $p < 0.05$ '+BFA' vs '-BFA'.

Fig. 9 KCNQ1 and KCNE1 are closer to each other on cell surface than inside cells. (A)

Experimental design. Live COS-7 cells coexpressing Q1-GFP and HA-E1-dsR were incubated with Q1 ext rabbit Ab and HA mouse Ab, followed by Alexa647 goat anti-rabbit and Alexa405 goat anti-mouse. Therefore, far red and blue fluorescence signals reported cell surface Q1-GFP and HA-E1-dsR. Green and red fluorescence signals reported total Q1-GFP and HA-E1-dsR. (B) Representative raw images of far red and blue channels (cell surface Q1-GFP and HA-E1-dsR), and green/red channels (cytoplasmic counterparts). The raw images were deconvolved, chromatic aberration corrected, and segmented to identify fluorescence foci. (C) Segmented images of the same cells, showing fluorescence foci. The coordinates of fluorescence foci were used to calculate the nearest neighbor distances. (D) Distribution of distances between nearest Q1-GFP neighbors to HA-E1-dsR on cell surface (top, far red foci to blue foci) and in cytoplasm (bottom, green foci to red foci) based on 22,648 and 47,119 nearest neighbor distances, respectively, from 10 cells. The median distances were 0.44 and 1.76 μm , respectively.

Fig. 10 Check the quality of immunoprecipitates from HEK293 cells before LC/MS-MS, and validate a novel Q1-GFP interactor (microtubule plus-end binding protein 1, EB1) identified in proteomic experiments. Two batches of HEK293 cells (Exp #1 and Exp #2) transfected with Q1-GFP and HA-E1-dsR, and one batch of untransfected HEK293 cells (-cDNA) were lysed in 1% Triton X-100 lysis buffer. Protein concentrations of whole cell lysates (WCL) were adjusted to 7.6 $\mu\text{g}/\mu\text{l}$. Three equal fractions of WCL (900 μg each) from each of the three (-cDNA, Exp #1, Exp #2) were subject to immunoprecipitation with dsR rabbit Ab, GFP rabbit Ab and GFP goat Ab. (A) Immunoblot analysis of WCL and immunoprecipitates. WCL lanes were loaded 15 μg protein each. IP lanes were loaded 5% of the total immunoprecipitates (i.e. IP from equivalent to 45 μg WCL). After SDS-PAGE and protein transfer to PVDF membrane, the membrane was cut below the 75 kDa size marker (SM) band. The upper portion was probed with GFP goat Ab (WCL and IP with rabbit Abs) or GFP rabbit Ab (IP with GFP goat Ab). The lower portion was probed with HA mouse Ab. (B) Test native EB1 protein in immunoprecipitates with GFP rabbit Ab (left) and dsR rabbit Ab (right). WCL and three lanes for each IP reaction (Super = WCL after IP, [-] IP without Ab, [+] IP with Ab) were fractionated by SDS-PAGE. After proteins were transferred to PVDF membrane, the membrane was cut below 75 kDa size marker band. The upper portion was probed with GFP goat Ab. The lower portion was first probed with HA mouse Ab, and after stripping, reprobed with EB1 rat Ab. The green and red arrows point to expected Q1-GFP bands (100 kDa and 200 kDa, monomer and dimer) and HA-E1-dsR bands (42 kDa if

unglycosylated, higher molecular weights if N- and/or O-glycosylated (Chandrasekhar *et al.*, 2011)). Native EB1 migrated as monomer and dimer (30 and 60 kDa, respectively) (Chen *et al.*, 2014).

Fig. 11 Microtubule plus-end binding protein 1 (EB1) binds KCNQ1 and promotes its surface expression. (A) Rat ventricular myocytes transduced with Q1-GFP and HA-E1-dsR were cultured for 36 hr and used for two types of experiments. 'a' *Coimmunoprecipitation*: Three equal aliquots of myocyte whole cell lysate (WCL, in 1% Triton X-100) were incubated with immunoprecipitating (IP) antibodies: GFP rabbit Ab, HA mouse Ab, and EB1 rat Ab, in the presence of protein A/G beads. WCL, negative control ([−], WCL incubated with protein A/G beads without IP Ab) and positive immunoprecipitate ([+]) were fractionated by SDS-PAGE. Proteins were transferred to PVDF membrane, and the membrane was cut below the 75 kDa size marker. The upper portion was probed with GFP goat Ab and the lower portion was probed with dsR rabbit Abs (listed on the left). After ECL, the lower portion was stripped and reprobed with EB1 rat Ab. For illustration purpose, irrelevant bands were removed. EB1 monomer and dimer bands are noted as 1x and 2x. Q1-GFP and native EB1 dimer co-immunoprecipitated reciprocally (marked by \$). HA-E1-dsR and Q1-GFP co-immunoprecipitated reciprocally (marked by * and #). However, there was no sign of co-immunoprecipitation between HA-E1-dsR and EB1. 'IgG': GFP rabbit Ab heavy chain detected by the secondary goat anti-rabbit Ab. 'b' *immunofluorescence/confocal microscopy*: Fixed myocytes without membrane permeabilization were incubated with Q1 ext rabbit Ab to label cell surface Q1. After membrane permeabilization, myocytes were incubated with GFP mouse Ab (binding total pool of Q1-GFP) and EB1 rat Ab (binding native EB1), followed by Alexa568-, Alexa488- and Alexa647-conjugated secondary Abs targeting rabbit, mouse and rat Abs, respectively. Shown are representative images from a myocyte at cell center and close to top surface, acquired with Zeiss 880 in the Airyscan mode. (B) COS-7 transfected with Q1-GFP alone or with EB1-dTomato. Confocal images show that Q1-GFP expressed alone stayed in the ER. However, with EB1-dTomato overexpression Q1-GFP overlapped with EB1-positive structures and reached the plasma membrane.

Fig. 12 Search for KCNQ1 and KCNE1 interactors in their trafficking paths. (A) Venn diagram of proteins found in KCNQ1-GFP immunoprecipitate (109 proteins) and in HA-KCNE1-dsR immunoprecipitate (109 proteins). Sixty eight are shared. (B) Manually curated list of proteins involved in membrane protein trafficking uniquely found in KCNQ1-GFP IP, HA-KCNE1-dsR IP, or shared between the two. (C) Cartoon of KCNQ1 and KCNE1 forward trafficking, assembly and endocytosis.

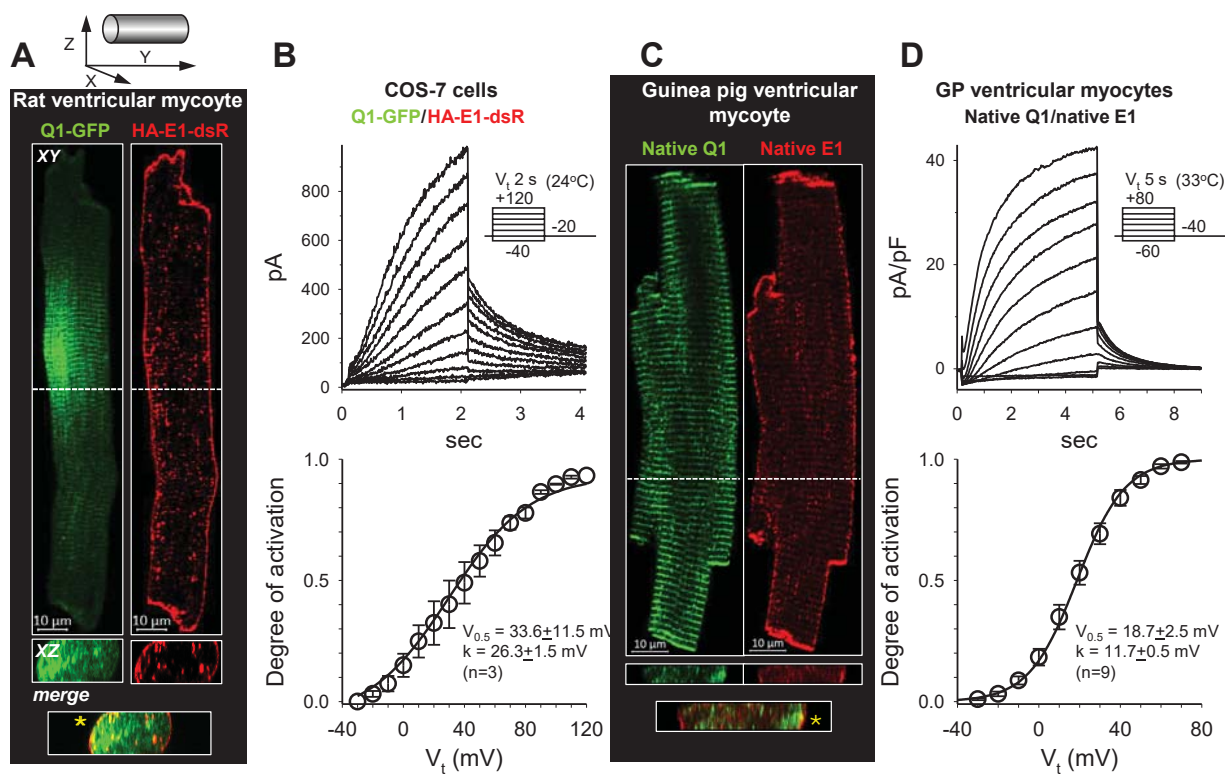


Fig. 1

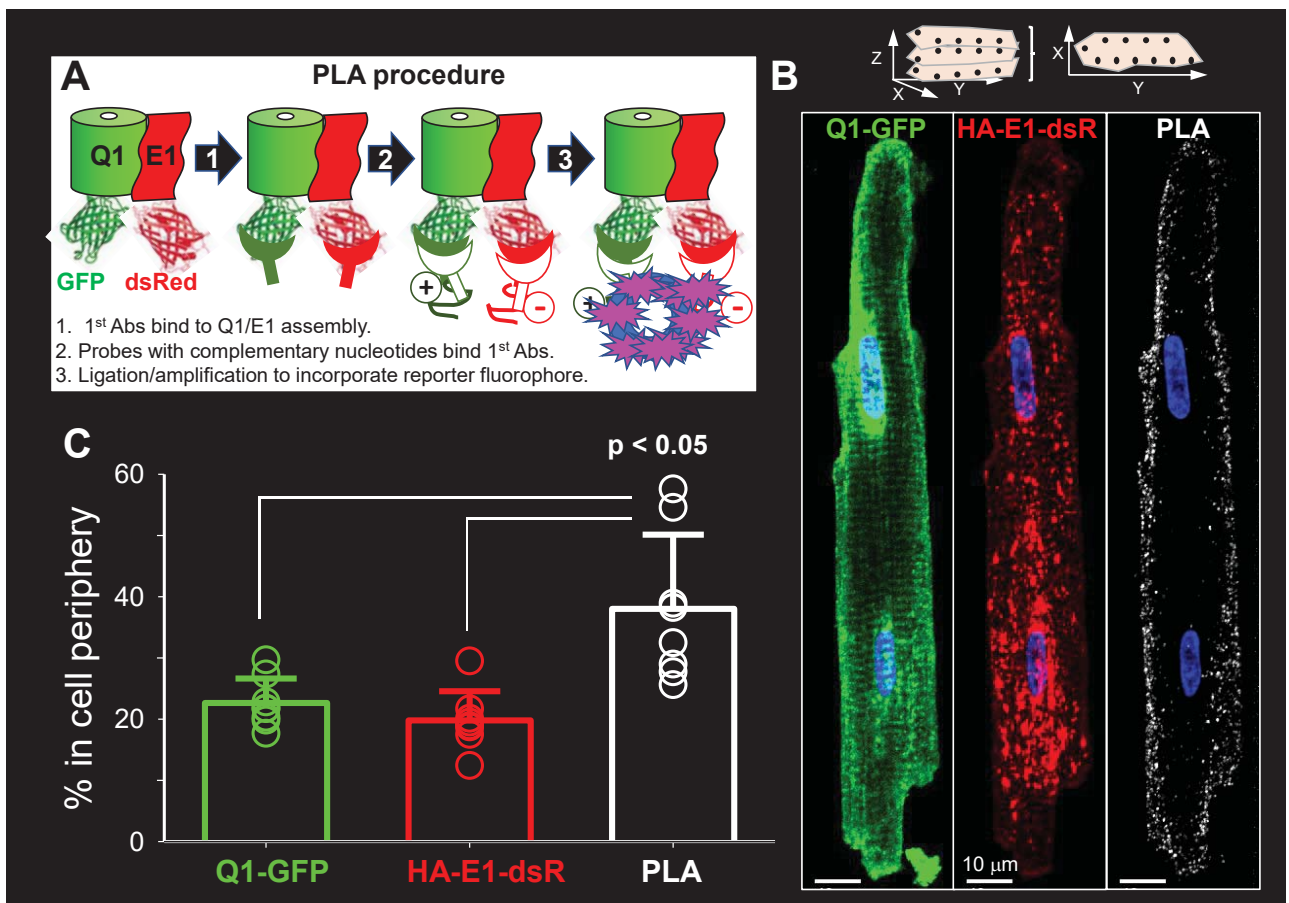


Fig. 2

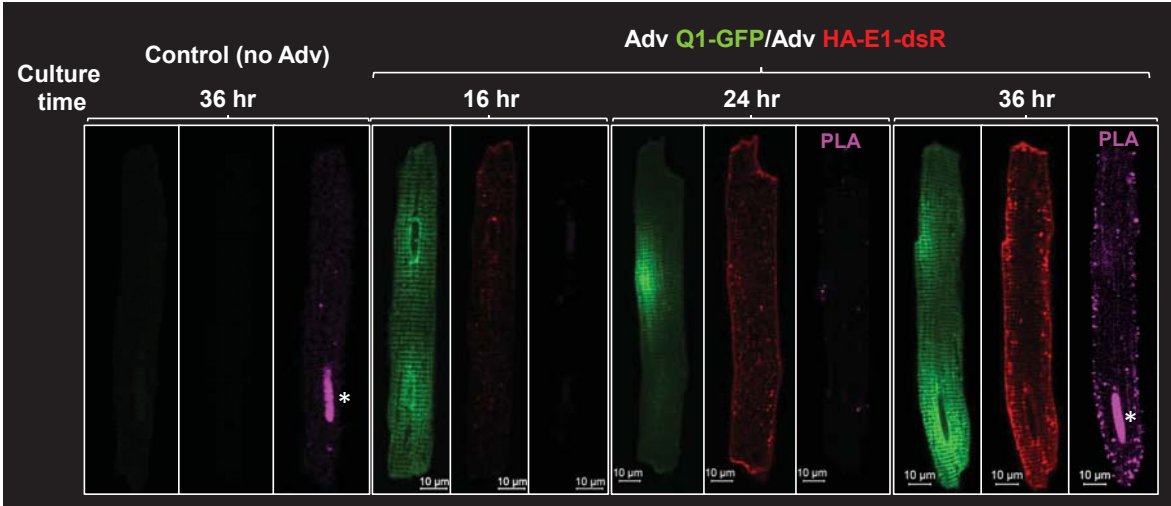


Fig. 3

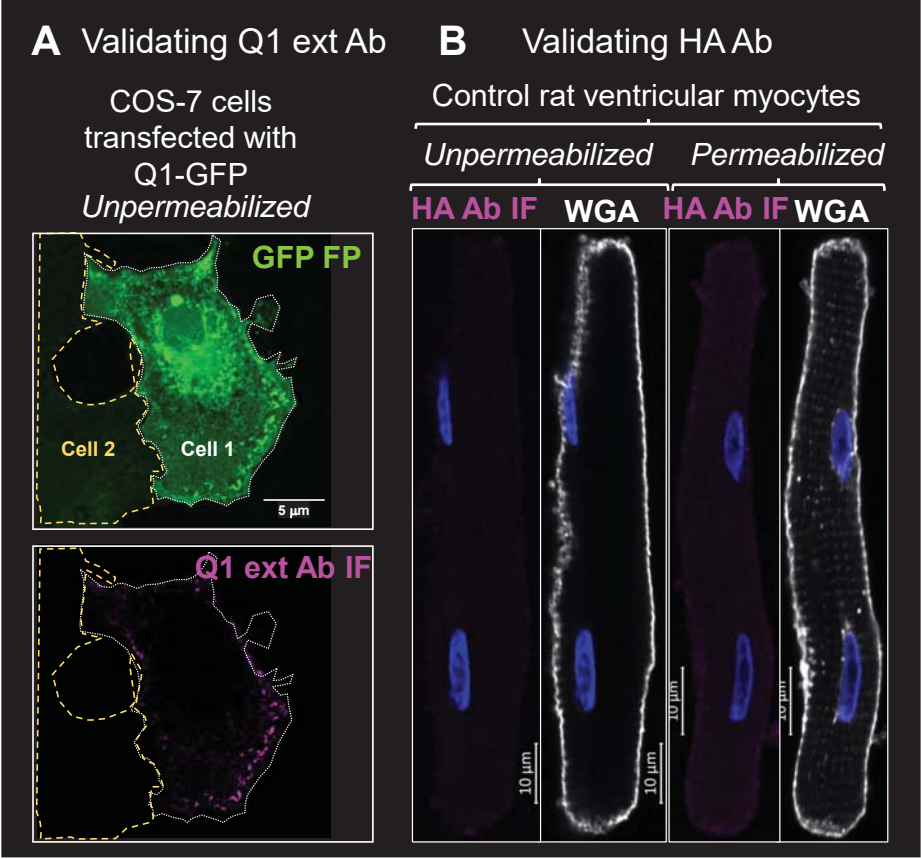


Fig. 4

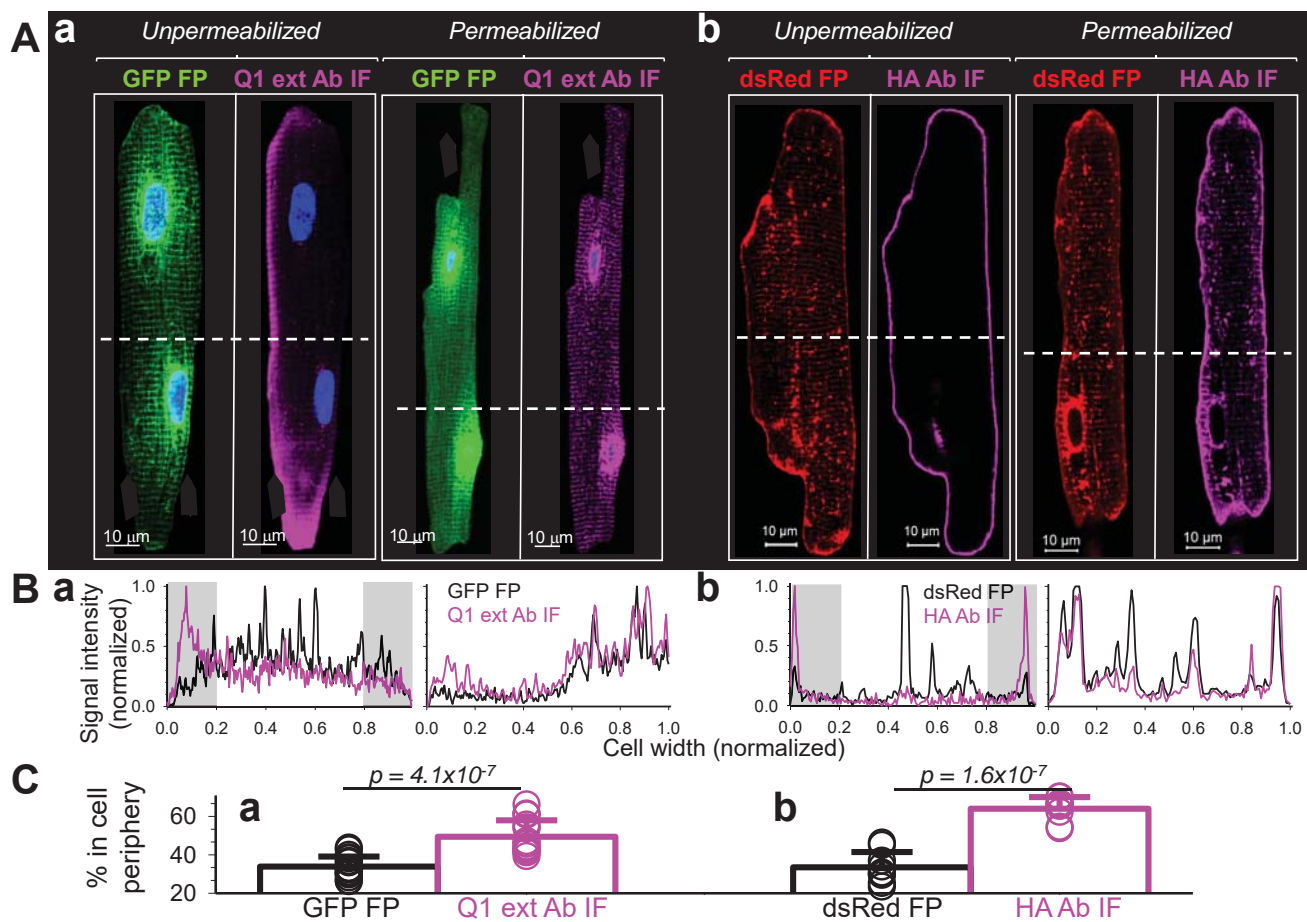


Fig. 5

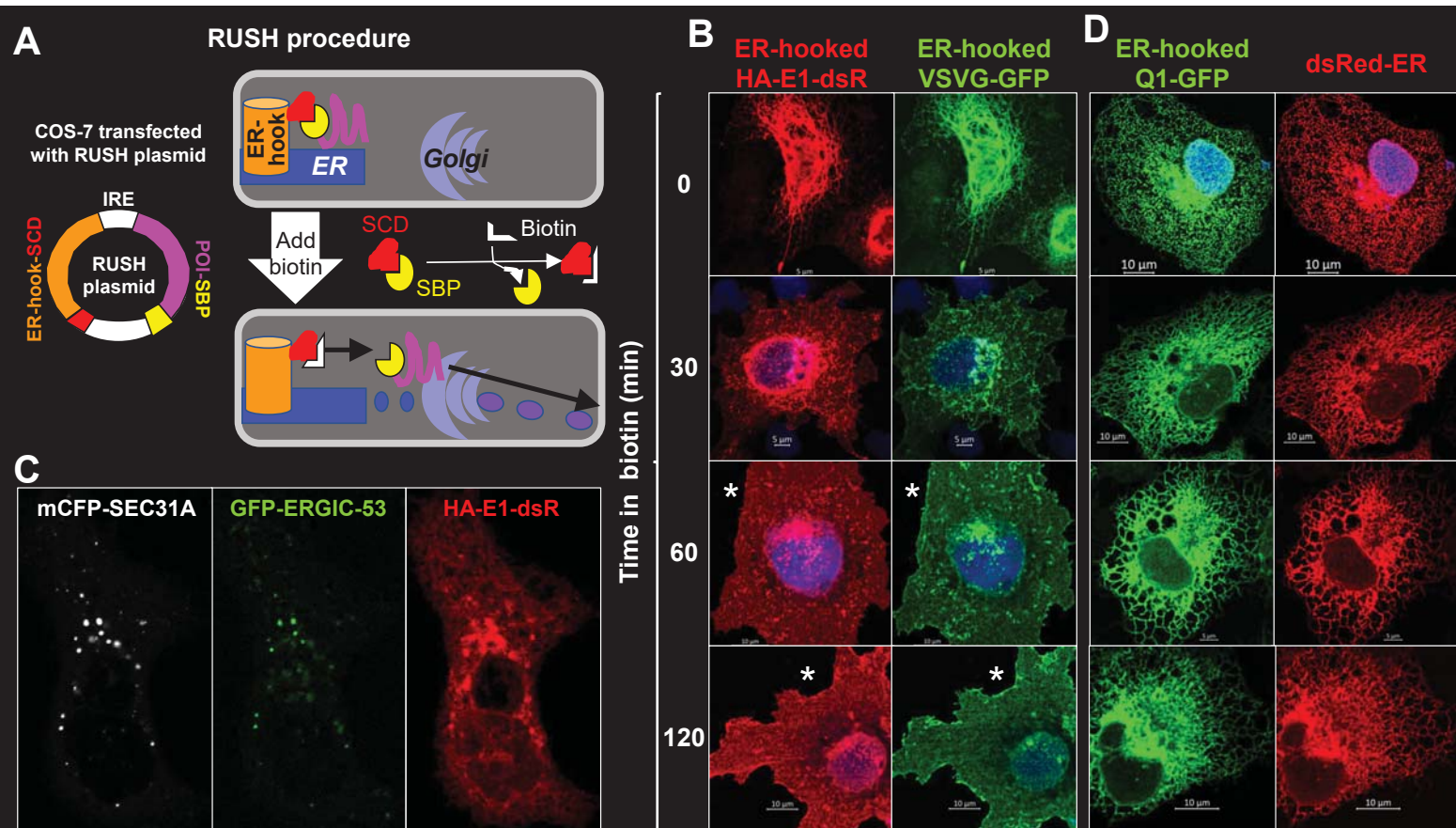


Fig. 6

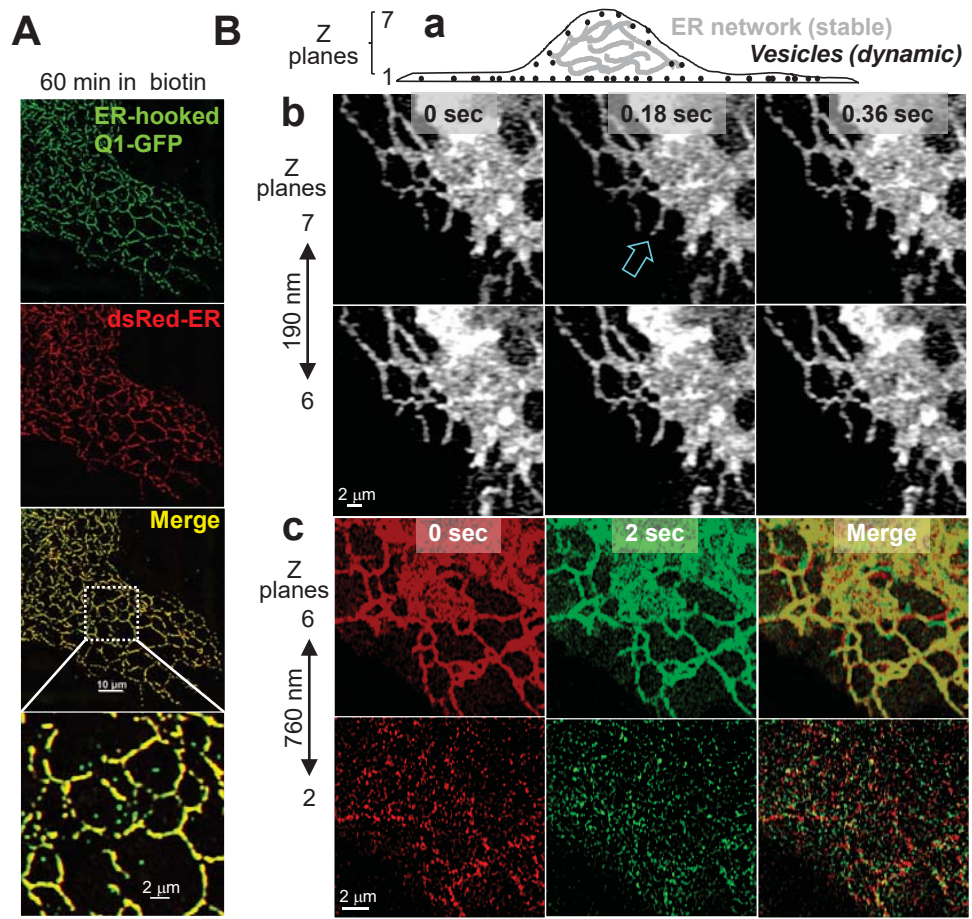


Fig. 7

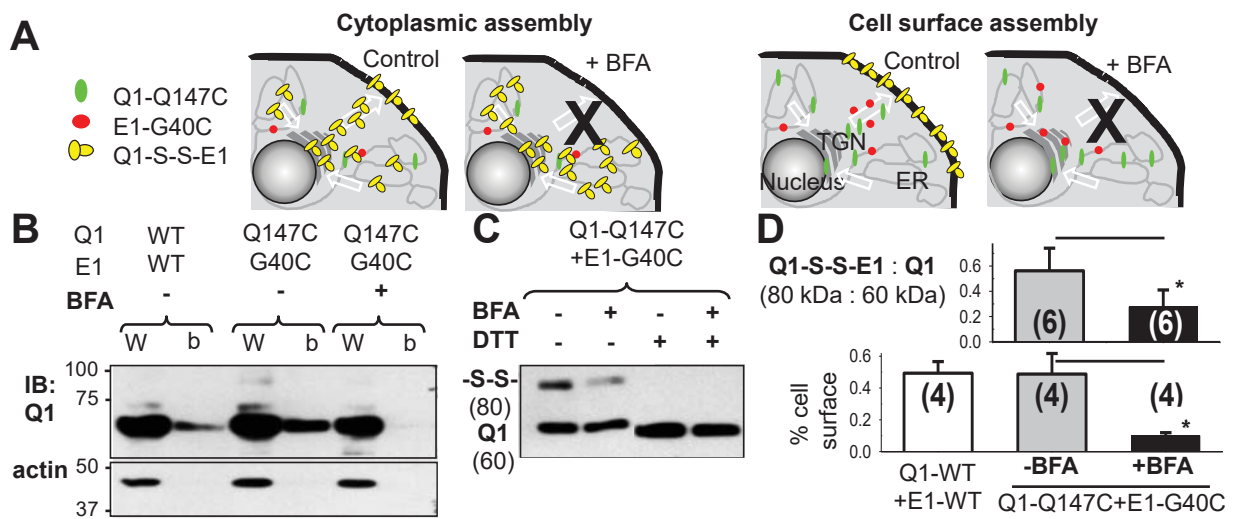


Fig. 8

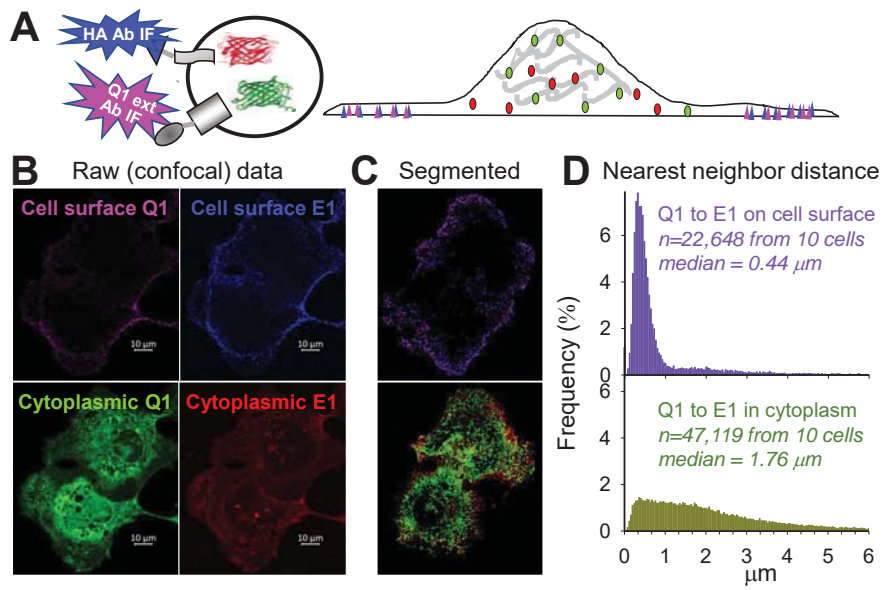
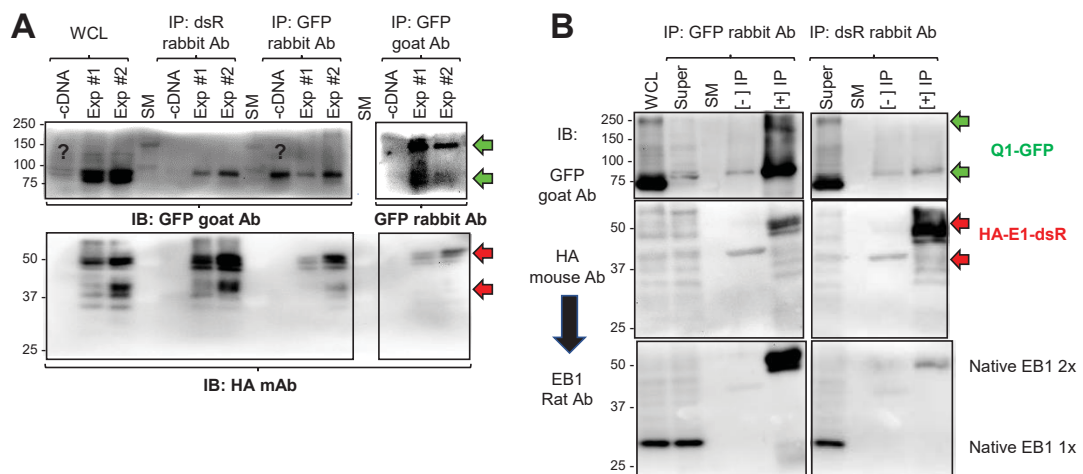


Fig. 9



Based on HEK exp/IP 191102, WCL = 7.6 ug/ul, load 13.5 ug/lane
 IP of 900 ug WCL and elute into 80 ul, use 4 ul in IB, equivalent to 45 ug WCL

Fig. 10

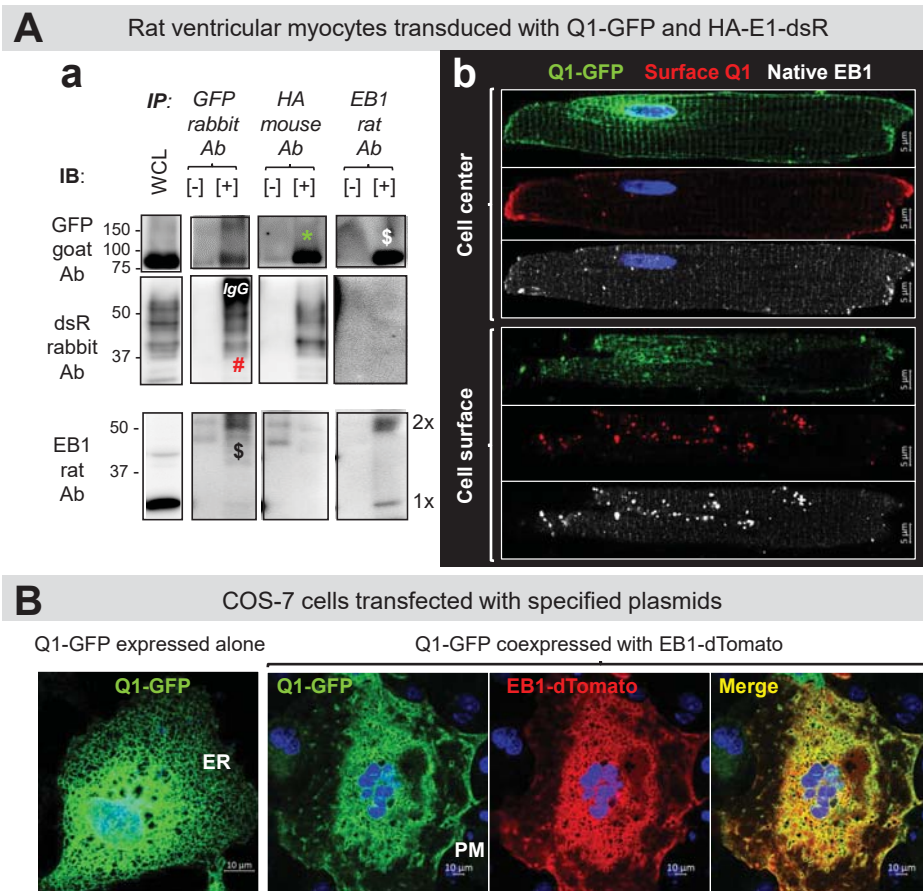


Fig. 11

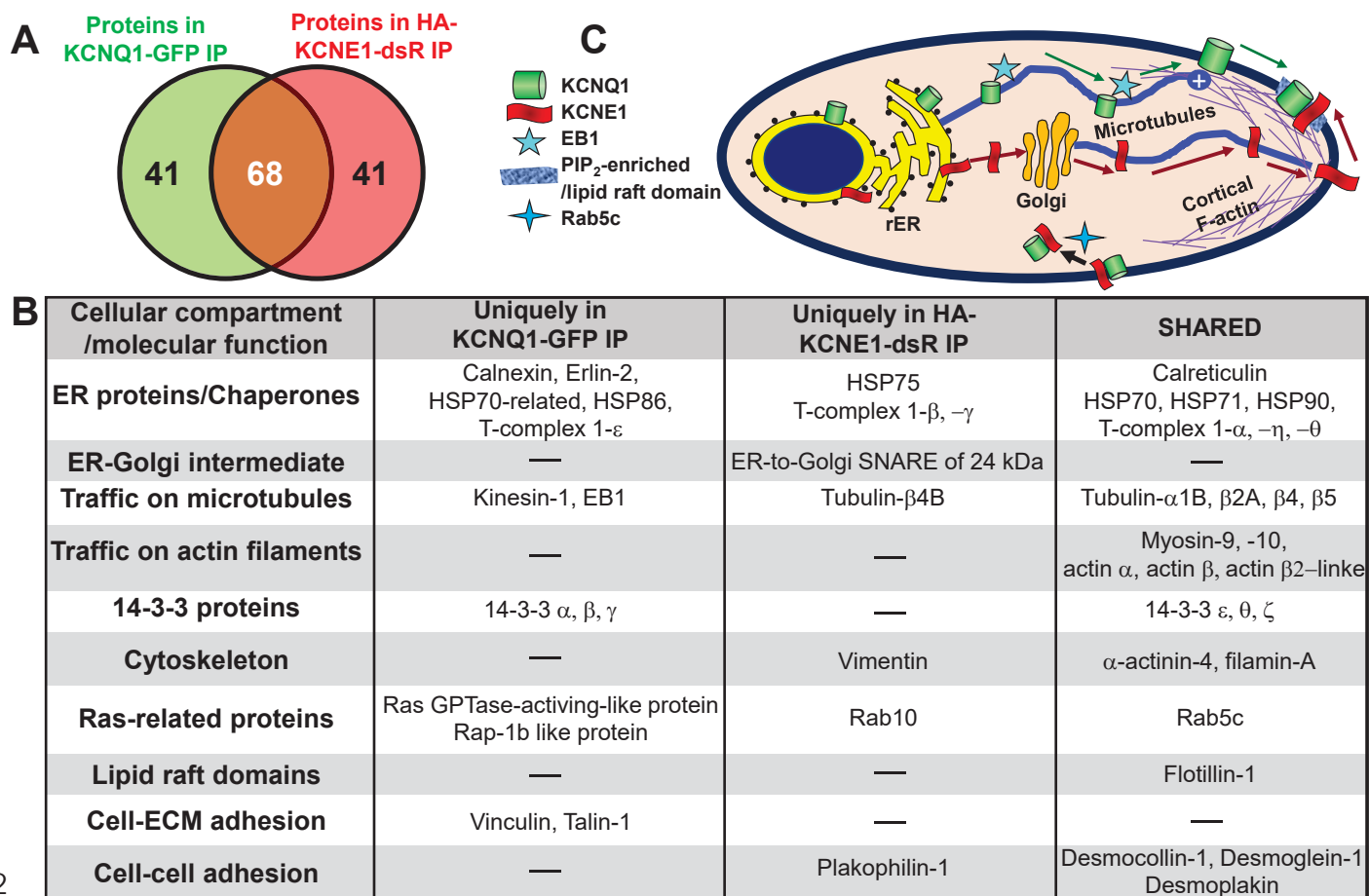


Fig. 12